



Modelling climate change impact on soil erosion in a watershed of north-western Lesser Himalayan region

K. R. Sooryamol¹ · Suresh Kumar² · Mary Regina³ · Anu David Raj¹

Received: 26 October 2021 / Revised: 12 January 2022 / Accepted: 13 January 2022 / Published online: 3 February 2022
© The Author(s), under exclusive licence to Springer Nature Switzerland AG 2022

Abstract

The fragile and immature soils in the sloping terrain of the Himalayan landscape is susceptible to soil erosion. Besides this, climate change may significantly enhance the soil erosion. Policymaking needs reliable estimation of the soil erosion to suggest suitable conservation measures. Hence, keeping this in view, the study was carried out to simulate climate change impacts on soil erosion for a small watershed of Lesser Himalayan region employing calibrated SWAT model. The model was calibrated and validated using the observed surface runoff and sediment yield data obtained from the watershed gauging station. The SWAT model performed well in estimating surface runoff ($r^2=0.85$) and sediment yield ($r^2=0.86$) with high model Nash–Sutcliffe Efficiency (NSE) for surface runoff (NSE=0.81) and sediment yield (NSE=0.70). The highest average soil loss was estimated from the scrubland (42.8 tons ha⁻¹ year⁻¹) and the least from the moderately dense forest (20.1 tons ha⁻¹ year⁻¹) during the current period. Subsequently, the calibrated SWAT model simulated to predict soil erosion in future. MarkSim DSSAT weather generator is a web-based tool used to obtain future climate scenarios. The downscaled General Circulation Model (GCM) projections were obtained from the MarkSim DSSAT weather generator tool. These projections Representative Concentration Pathway (RCP) 4.5 and 8.5 indicated an increase in rainfall depth of 12.3–14.2%. The predicted soil erosion revealed an increase in annual soil erosion rate from 18.1 to 20.9% under various emission scenarios during the twenty-first century. The outcomes exposed that climate change may increase the variability and rates of soil erosion by increasing rainfall intensities and depths. The comprehensive information generated from the study will help the government and policymakers to suggest suitable conservation measures in preparing sustainable land use plan in the Himalayan region.

Keywords Surface runoff · Sediment yield · SWAT model · Climate change adaptation · Himalayas · RCP scenario

Communicated by M. V. Alves Martins

✉ K. R. Sooryamol
sooryamolkr96@gmail.com

Suresh Kumar
suresh_kumar@iirs.gov.in

Mary Regina
maryregina.f@kau.in

Anu David Raj
anudraj2@gmail.com

¹ College of Climate Change and Environmental Science (CCCES), Kerala Agricultural University, Thrissur, Kerala, India

² Agriculture and Soil Division, Indian Institute of Remote Sensing (IIRS), Indian Space Research Organisation (ISRO), Dehradun, Uttarakhand, India

³ College of Agriculture, Kerala Agricultural University, Thrissur, Kerala, India

1 Introduction

Soil erosion is considered as most serious concern of land degradation process around the world. It adversely affects the physicochemical properties of soils and agricultural productivity in a landscape (Lal, 2003; Pimentel, 2006). It is a complex process comprised of the splash, sheet, rill, and gully forms of erosion, resulting in the removal of top fertile soil and terrain deformation (Ballabio et al., 2017). It will adversely affect the services provided by soil ecosystem and thereby food security.

According to GSP (2017), every year 75 billion tons of soil eroded from agricultural land with an estimated economic loss of US\$400 billion year⁻¹. In India, nearly 120.7 million hectares of land have been degraded, and water erosion accounting for 70% (NAAS, 2012). Borrelli et al., (2017) stated that the expansion of agricultural land leads to enhanced soil erosion rates in southeast Asia. The

developing countries are facing the highest rate of soil erosion, and found a lower reduction of soil erosion by adopting soil and water conservation measures as compared to developed countries. They also reported that 7.6% of the total land area in India is above the soil tolerable erosion limit ($10 \text{ tons ha}^{-1} \text{ year}^{-1}$). The rate of soil erosion in India ranged from low ($< 5 \text{ tons ha}^{-1} \text{ year}^{-1}$), in the dense forest, to high ($> 80 \text{ tons ha}^{-1} \text{ year}^{-1}$), in the Shiwalik hills (e.g. David Raj et al., 2021; Singh et al., 1992; Swarnkar et al., 2018). Wuepper et al. (2020) also reported that annually India faces a high rate of soil erosion ($> 40 \text{ t h}^{-1}$). The Himalayan region of India witnesses severe erosion as it receives high rainfall amount and weak geological formation, active seismicity, immature, and fragile soil types with poor agricultural management practices (Tiwari, 2008). George et al. (2021) identified that, in Uttarakhand, 20.3% of the region is under critical soil erosion, which reaches values higher than $40 \text{ tons ha}^{-1} \text{ year}^{-1}$.

Over the last few years, remote sensing and geographic information systems (GIS) have developed a vital tool for generating spatially distributed land use/land cover (LULC), topography, and soil properties in the watershed (Kebede et al., 2021; Pijl et al., 2020). Applications of remote sensing and GIS techniques serve as vital tool to estimate the spatial distribution of soil erosion severity. The spatial distribution of soil erosion risk assessment provides the severity of soil erosion of the watershed in various time period. The universal soil loss equation (USLE) (Jemai et al., 2021), revised universal soil loss equation (RUSLE) (Islam et al., 2020), and modified universal soil loss equation (MUSLE) (Gwapedza et al., 2021) are used most commonly for predicting soil erosion. While the physically based model can provide a more reliable and realistic output after the calibration and validation using the site-specific soil erosion factors and measured data. Soil and Water Assessment Tool (SWAT) is a physically based hydrological model extensively explored to simulate the surface runoff and sediment yield from the watershed/catchment scale (Briak et al., 2019; Zhang et al., 2020; Shi and Huang, 2021). These models partition the watershed into hydrological response units (HRUs) for accounting the spatially distributed factors affecting soil erosion and sediment yield. These techniques allow the identification of the highest soil erosion units and to analyse the consequence of different land use and management methods for preventing soil erosion (Boufala et al., 2021; Mosbahi & Benabdallah, 2020; Osei et al., 2019). SWAT has been widely used for runoff and sediment studies in the small and large catchments around the different regions of the globe (Azair et al., 2016; Sisay et al., 2017; Himanshu et al., 2019; Hu et al., 2020; Kuti & Ewemoje, 2021; Kwarteng et al., 2021). Abbaspour et al. (2015) provide detailed description of SWAT model calibration and validation procedures for the large scale.

Often, climate change is expected to play a substantial role in enhancing soil erosion in the future. The Himalayan landscape is the most complex mountain environment and is extremely sensitive to global warming (Tewari et al., 2017). Soil erosion is expected to increase by 9% because of climate change, during the twenty-first century (Yang et al., 2003). Doetterl et al. (2012) stated that the rainfall erosivity and steep slope significantly contribute to the soil erosion in hilly and mountainous terrain. Steep slopes and torrential high-intensity rainfalls are the characteristics of the Himalayan region. The change in Himalayan ecosystem will have global consequences. Kumar et al. (2015) found that rainfall in the Himalayan region increases at a strong positive trend. The variation of rainfall patterns because of climate change might bring a higher rate of soil erosion. The climate models provide a unique opportunity to simulate soil erosion and sediment loss by integrating the future climate change scenarios (Awar & Khare, 2020; Luetzenburg et al., 2020; Maurya et al., 2021; Saharia & Sarma, 2018; Salazar et al., 2012). However, the main problem lies with the coarse resolution of global climate models (Rivington et al., 2008; Samaras & Koutitas, 2014). The reliable simulation requires the downscaling of coarse resolution climate change scenarios into finer resolution. MarkSim DSSAT weather generator is a web-based tool used to obtain future climate scenarios. It provides the downscaled climate data for the future rainfall on a daily timescale (Raisi et al., 2021; Trotochaud et al., 2016). Alam et al. (2021) and Ficklin et al. (2009) utilised the SWAT to predict the hydrology and impact of climate change over the watershed and river basins. Furthermore, Kumar et al. (2016) evaluated the functioning of SWAT and SWAT-VSA for surface runoff generation in a Himalayan watershed of Uttarakhand and found it simulating satisfactorily.

According to Gupta et al. (2019), the socio-ecological condition of the Himalayas is degrading due to climate change and also has a potential for further intensification. The soil erosion and decreased soil moisture content are severe problems in the hilly and mountainous region which directly affect the livelihood of native peoples. The zone-specific adaptation and mitigation policies are more effective in these scenarios. However, the lack of monitoring and evaluation method is a significant constraint in the hilly and mountainous region. Borrelli et al. (2021) reported that the soil erosion in Indian Himalayas is high, although there are fewer soil erosion measurement sites (sediment gauging stations) are present as per García-Ruiz et al. (2015). Moreover, Alewell et al. (2019) stated that the scientific community widely accepts only the calibrated and validated models because of the uncertainty of the modelling approach. In India, majority of the studies identified the soil erosion and climate change impact on soil erosion using the empirical models (Bagwan & Gavali, 2021; Chakraborty et al., 2020;

Ganasri & Ramesh, 2016; Mondal et al., 2015; Pal et al., 2021; Prasannakumar et al., 2012) where the calibration and validation of these models were lacking. Only few studies were conducted using physically based soil erosion models due to the lack of a measured/gauging data in India. While in this study, we attempted to simulate the future soil erosion scenario using the calibrated SWAT model based on the IPCC emission scenarios (RCP 4.5 and 8.5), which gives a more reliable future soil erosion quantification than the uncalibrated models. It will be more beneficial for the farmers, local planners, policymakers, and to the Governments.

Thus, the current study is carried out in an experimental watershed located in Uttarakhand, India. No such study has been attempted to simulate the climate change scenarios with calibrated model parameters in the north-western Lesser Himalayas. The study was carried out to simulate climate change impact on calibrated SWAT model parameters in predicting soil erosion for small watershed. The SWAT model was calibrated for small watershed with measured data of surface runoff and sediment yield on daily weather data for the years 2016–2018. It aims to (i) calibrate and validate the SWAT model using the measured data from the instrumental watershed to assess its applicability and performance in a humid subtropical region; (ii) simulate the baseline soil loss relating to different land uses, and (iii) simulate future soil loss using the IPCC—RCP emission scenarios (4.5 and 8.5).

2 Study area description

The Pasta watershed (a part of Sitla Rao watershed located in Dehradun, Uttarakhand) is extending from 30° 27' to 30° 28' North latitude to 77° 54' to 77° 55' East longitude, encompassing an area of 57 hectares representing the Lesser Himalayan topography, which belongs to the Garhwal Himalayas (Fig. 1). Elevation of the study area ranges from 835 to 1374 m. Soils in the study area are derived from the alluvium parent material. Inceptisols are the major soil classes found in the experimental site, with textures varying from sandy loam to loam.

The major land use units occupying the study area are forest, agricultural land (maize and paddy), scrub land, and settlements. The western part of the study area contains moderately dense to dense Sal (*Shorea robusta*) forest. According to Koppen and Geiger (2007), climate classification the study area comes under the humid subtropical climate (Cwa). The watershed has three significant seasons; the hot summer season from March to June, the wet monsoon season from July to September and the cold winter season from October to February. The average annual temperature ranges from 15.8 to 33.3 °C. The hottest month, May, experience a maximum average temperature of 35.3 °C, and the

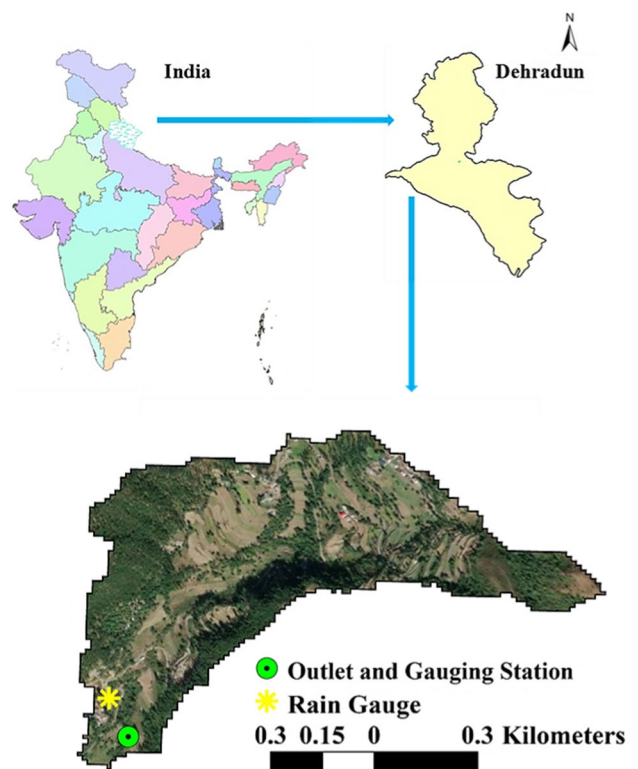


Fig. 1 Location of the study area

coldest month, January, has a minimum average temperature of 3.6 °C. The average annual rainfall is 2245.1 mm, and most of the rainfall was received from July to October (Singh et al., 2021).

3 Materials and methods

The detailed methodology flowchart of the study is illustrated in Fig. 2.

3.1 Data used

3.1.1 Satellite data

The Cartosat Digital Elevation Model (DEM) (10 m) and Resourcesat-2 multiband LISS IV (5.8 m) were the major satellite products used in this study. The DEM was used to identify the topographical parameters such as slope, steepness and drainage network. LISS IV false colour composite was utilised for the LULC map generation. The spatial analysis was carried out using the spatial analyst module of the ArcGIS 10.3 version software. The Cartosat DEM, slope, and LULC maps were utilised as the SWAT model's primary input raster maps.

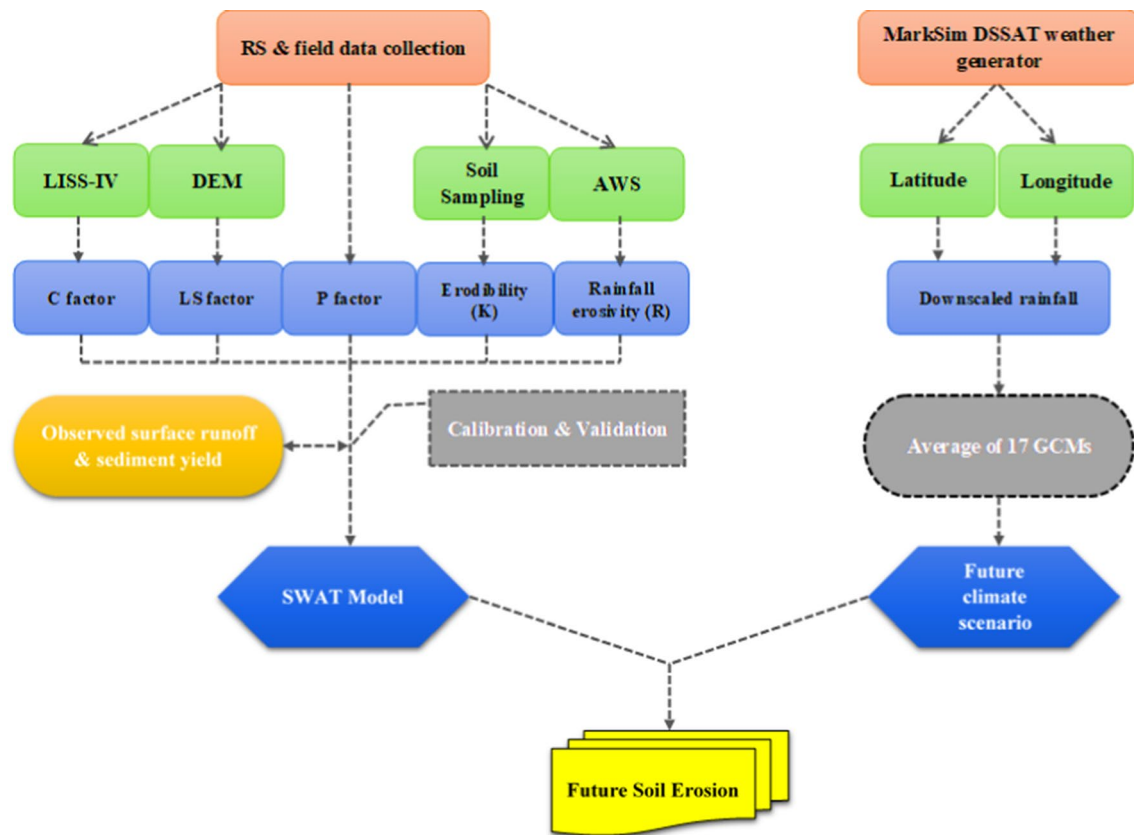


Fig. 2 Methodology of study. Legend: *RS* Remote Sensing, *DEM* Cartosat Digital Elevation Model, *LISS IV* Linear Image Self Scanner, *AWS* Automatic Weather Station, *C factor* Cover factor, *LS factor*

Slope Length and Slope factor, *P factor* Practice factor, *GCM* General Circulation Models

3.1.2 Field data collection and soils map

Soil samples were collected for the surface (0–15 cm) and sub-surface (16–30 cm) from the various soil-landscape units during 2018–2019. Soil sampling was conducted based on the transect method, and the associated locations of sampling sites were georeferenced using the Global Positioning System (GPS) (Fig. 3). The soil samples were analysed to find soil texture, bulk density, pH, electrical conductivity, and organic matter. During the field survey, erosion features and other site-specific characteristics were also identified. The infiltration rate and unsaturated hydraulic conductivity were measured using a mini-disk Infiltrometer. LULC data were gathered, and their geographic position was determined using GPS. Additionally, land management methods in the watershed were collected to define the SWAT model's management practise component (*P factor*). Maize and paddy are the primary rainy season's crops (July–October). Thus, between July and October 2018, average plant height and density data were collected at 30-day intervals from ten randomly selected fields with a plot size of 1–2 m² from the experimental watershed. These data were used to create crop

parameters such as maximum and minimum crop height, crop density, and defining the crop life cycle stages for the SWAT model.

3.1.3 Weather data, surface runoff, and sediment yield measurement

The weather data from 2016 to 2018 were received from the rain gauge and Automatic Weather Station (AWS) installed by Indian Institute of Remote Sensing, Indian Space Research Organisation (ISRO), Dehradun near the watershed outlet. The rainfall, maximum, and minimum temperature are the major parameters needed for the simulation of the SWAT model. Solar radiation, relative humidity, and wind speed data are the other parameters. The rainfall and temperature data during the monsoon period (July to October) were considered for the model calibration and validation. The rainfall during the rest of the months were negligible and did not contribute sediment samples from the sediment tank. Moreover, the rainfall data from 1986 to 2015 collected from India Meteorological Department (IMD) used for identifying the average rainfall over the base period.

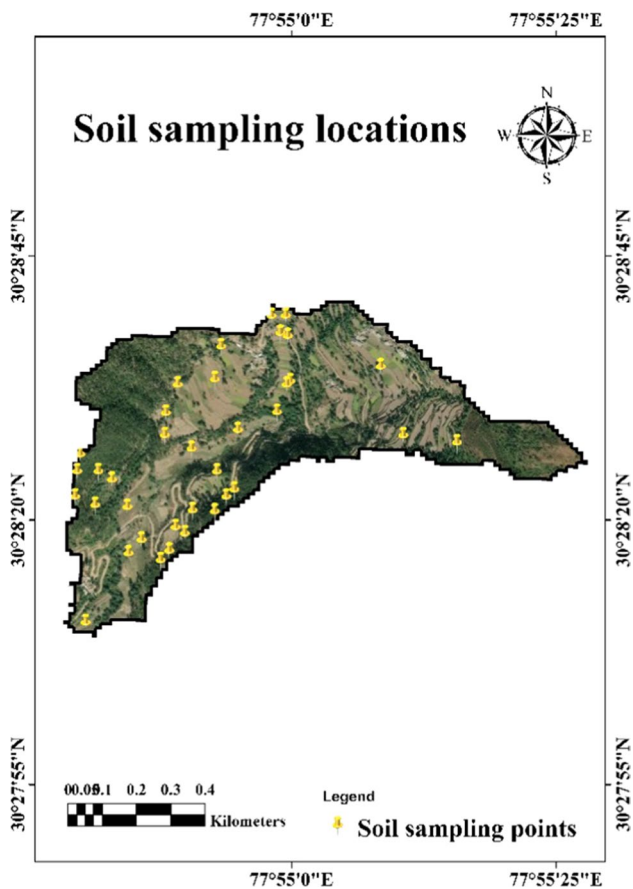


Fig. 3 Soil sampling locations

The daily surface runoff data and sediment yield samples collected from the gauging station constructed at the watershed outlet (Fig. 4). It consists of a weir structure (Fig. 4a and b) fitted with a digital water level recorder (Fig. 4c) and sediment sampling tank. It collects daily surface runoff at a 15-min frequency from a 57 ha catchment area. A perforated steel pipe is fitted at the middle of the weir structure connected to the sediment tank. A 500-litre (sediment sampling tank (Fig. 4d)) was built near the outlet for collecting the runoff water continuously during the rainfall. After the rain, every day at 08:00 h (IST), the runoff water sample from the sediment tank was collected in a 1-litre bottle representing the runoff water sample on the cumulative basis of the day. Sediment concentration was estimated in the laboratory after filtering and drying the sediments from the runoff water sample. After that, total sediment washed from the outlet was computed based on the total daily discharge (runoff water).

3.2 SWAT model description

SWAT was developed by Dr Jeff Arnold (Neitsch et al., 2011) as part of the USDA Agricultural Research Service’s (ARS) 30-years modelling expertise (Gassman et al., 2007). SWAT is a physically based (Neitsch et al., 2011) model that executes daily basin-scale simulations. The model is computationally efficient and capable of simulating the influence of management on water, sediment, and chemical yields using readily available inputs (Neitsch et al., 2011). Additionally,

Fig. 4 Instrumented gauging site at the watershed outlet: stilling well (a), weir structure (b), digital water level recorder (c), and sediment sampling tank (d)



the SWAT can be used to model a watershed in the absence of gauge data (Gassman et al., 2007; Neitsch et al., 2011). SWAT partitions the watershed into several sub-watersheds or sub basins and subdivided into hydrologic response units (HRUs) with different land use, soil, and management characteristics. The model required the observed daily rainfall, maximum and minimum temperature, solar radiation, relative humidity, and wind speed data.

3.2.1 Runoff modelling

Using the SCS-CN (curve number) approach, the SWAT model simulates surface runoff volumes for each HRU (USDA-SCS 1972).

$$Q = (R - Ia)^2 / (R - Ia) + S, \quad (1)$$

where Q is the runoff (mm), R is the rainfall amount (mm), S is the retention parameter, and Ia is the initial abstraction, which is based on surface storage, interception, and infiltration (mm).

$$S = 25.4 (1000/CN - 10). \quad (2)$$

3.2.1.1 Peak runoff rate The peak runoff rate of the given rainfall event is the maximum runoff flow rate of that event, and it is used to estimate sediment loss and is an indicator of the erosive power of rainfall. SWAT uses the modified rational method to estimate the peak runoff rate.

$$Q_p = C * I * HRU_{area} / 3.6, \quad (3)$$

where Q_p represents the peak runoff rate (m^2/s), C represents the runoff coefficient, and I represents the rainfall intensity (mm/hr), the ' HRU_{area} ' (Km^2) in the area of HRU, and 3.6 is the area conversion factor.

3.2.2 Sediment yield modelling

The MUSLE was used in SWAT to estimate erosion caused by rainfall and runoff. MUSLE predicts the erosion rate as a function of erosion runoff component.

$$Y = 11.8 * (Q * Q_p * HRU_{area}) * 0.56 K_{usle} * C_{usle} * P_{usle} * LS_{usle} * CFRG, \quad (4)$$

where the sediment loss is denoted by the letter Y (metric ton), the surface runoff is measured in millimetres (mm), the peak runoff rate is measured in metres square per second (m^2/s), the HRU area is measured in square metres (ha), the USLE soil erodibility factor is K_{usle} , the cover and management factor are C_{usle} , the support practise factor is P_{usle} , the topography component is LS_{usle} , and the coarse fragment factor is 'CFRG'. A detailed explanation of each parameter

and model description can refer from the SWAT theoretical documentation (Neitsch et al., 2011).

3.2.3 Creation of SWAT model hydrological response units (HRUs)

The SWAT model simulates surface runoff and sediment yield for each hydrologic response unit (HRU). HRU is defined in SWAT by combining LULC, management, and hydrologic soil group (HSG) obtained from the soil-landscape unit map (Neitsch et al., 2002). The Cartosat 10 m resolution DEM was used to delineate the watershed. The land use land/cover map was imported into the model and classified as moderately dense forest, agriculture (Paddy & Maize), and scrub land. The soil map of the study area was prepared based on physiographic land use unit and the slope classes were defined manually. The overlay option was used to merge three maps to derive the HRU feature class. The HRU defined based on dominant land use, soil, and slope category. The weather data from the AWS station were imported into the model and prepared weather database for the simulation. Then write SWAT input tables option used to create the default model parameters. The site-specific soil physical, chemical, and hydrological properties and other necessary land use parameters were entered in the edit model parameter section. A critical aspect of the modelling process was defining management practices for the various land use types. For major crops such as paddy and maize, the crop phenological stages data were collected, and the management practises (P) factor were assigned. The write command is available for building the SWAT table, and the simulation menu appears with options for changing the timeframe and running the SWAT simulation. The hydrological response unit based prediction will provide a more accurate representation of the runoff and sedimentation processes in the watershed.

3.2.4 Model calibration and validation

The ArcGIS interface was used to provide the collected and measured input parameters into the SWAT model (ArcSWAT). Daily runoff data and sediment data collected were used to perform hydrologic calibration. Identifying the critical parameters for calibration and validation is crucial in modelling (Ma et al., 2000). These parameters were identified using the sensitivity analysis. According to the Parsimony Principle (Trocine & Malone, 2000), only a few factors contribute for considerable variations in model outputs, whereas the majority of other parameters have little impact. Morris (1991) employed the One-factor-at-a-Time (OAT) technique for sensitivity analysis. In this approach, the variations in output are induced by changing one input factor while maintaining all other parameters constant. There is

a provision of the calibration process in the SWAT model either via manual or auto calibration tools (van Griensven & Bauwens, 2003; Van Liew et al., 2005). Calibration is done manually, and entails modifying the values of the model's input parameters to generate simulated results that fall within a certain range of the observed data. As the limited number of observed data were available for calibration and validation, manual calibration was preferred (Balascio et al., 1998). The manual calibration procedure suggested by Arnold et al. (2012) adopted here.

The calibration was performed by adjusting the sensitive parameters like curve number and available water content (AWC). In addition, crop management factor (USLE—C), crop practice factor (USLE—P), soil erodibility factor (USLE—K) and slope factor were adjusted for the sediment yield calibration. These parameters were changed through the trial-and-error method to compare the predicted values close to the observed values. The valuation of the model's performance was assessed using a regression plot of projected and observed runoff. Available data (surface runoff) of rainfall days (28) from the years 2016, 2017 and 2018 were utilised to calibrate (16) and validate (12) the surface runoff. Similarly, model performance was evaluated using a regression plot of predicted versus observed sediment yield. Available data (sediment yield) of rainfall days (22) from the years 2016, 2017, and 2018 were utilised to calibrate (12) and validate (10) the model for sediment yield simulation. The goodness of fit measured by the correlation coefficient (r) and determination coefficient (r^2), which measures how well is the variance of observed parameter simulated by the model (Krause et al., 2005). The average tendency of simulated data to be larger or smaller than their observed equivalents is measured by percent bias (PBIAS) (Gupta et al., 1999). The Nash–Sutcliffe model Efficiency (NSE) (Niazkar & Zakwan, 2021), root mean square error (RMSE), and PBIAS were also used to measure the model efficiency.

3.3 Obtaining projected rainfall

MarkSim DSSAT weather generator has been developed (Jones & Thornton, 2013) for an easier and faster platform to acquire downscaled future climate data from different General Circulation Models (GCMs) for different locations (Trotochaud et al., 2016). MarkSim DSSAT weather generator is an online web application that can provide the downscaled weather variables such as rainfall, maximum, and minimum temperature. It estimates daily rainfall based on a wet day's probability using the third-order Markov process. Downscaled data of daily rainfall based on the RCP 4.5 and RCP 8.5 scenarios were obtained for 2011–2095 by providing the latitude and longitude of the area of interest. It has 17 Atmosphere–Ocean General Circulation Models (GCMs), for reliable outcomes, the Inter-governmental

Panel on Climate Change (IPCC) recommends an average of these models for any impact studies (Wilby et al., 2004). Thus, an average of these models, namely BCC-CSM 1.1, BCC-CSM 1.1 (m), CSIRO-Mk3.6.0, FIO-ESM, GFDL CM3, GFDL ESM2G, GFDL ESM2M, GIS E2-R, GIS E2-R, HadGEM2-ES, IPSL-CM5A-LR, 12. IPSL-CM5A-MR, MIROC-ESM, MIROC-ESM-CHEM, MIROC 5, MRI-CGCM3, and NorESM1-M (Jones & Thornton, 2000, 2013) were used for this study. It averages the polynomial functions that drive the GCM differences, which resulting in downscaled weather data that is accurate for the average GCM. This average daily rainfall data are considered as future projected rainfall.

3.4 Generation of future soil erosion

The downscaled future climatic parameters of the intermediate (RCP 4.5) and higher (RCP 8.5) emission scenario from 2011 to 2095 were utilised to evaluate the rainfall change. SWAT model was used to analyse the probable influences of climate change on soil loss for the various LULC types in the watershed. Only the rainfall amount was changed according to the downscaled rainfall scenario, and all other parameters were kept constant for the SWAT model. The projected rainfall data are divided into 30-year periods: 2011–2040 (the 2020s), 2041–2070 (the 2050s), and 2071–2095 (the 2080s). Thus, it helps to understand the probable impact of rainfall on soil erosion during various periods of the twenty-first century.

4 Results and discussion

4.1 Terrain, land use/land cover, and soils map

Spatial layers were created for the SWAT model using the ArcGIS spatial analyst component for quantifying the soil loss from the watershed. Terrain analysis revealed that 4.81% area in the watershed is classified under gentle (< 10% slope), 33.33% area under moderate to moderately steep (11–30% slope) and 61.86% area under steep (> 30% slope) classes. Based on Strahler (1953) stream ordering method (Fig. 5a), six first-order streams, two second-order streams, and one third-order stream in the experimental watershed were identified. The gauging station was located in the third-order stream of the experimental site. A higher number of drainage networks in the watershed indicate a higher soil erosion rate. The LULC map (Fig. 5b) was prepared using ArcGIS software. The dominant LULC area is under maize, followed by moderately dense forest, paddy field and scrub/barren land, and which covers 38.4, 26.0, 24.4, and 8.9% of the watershed.

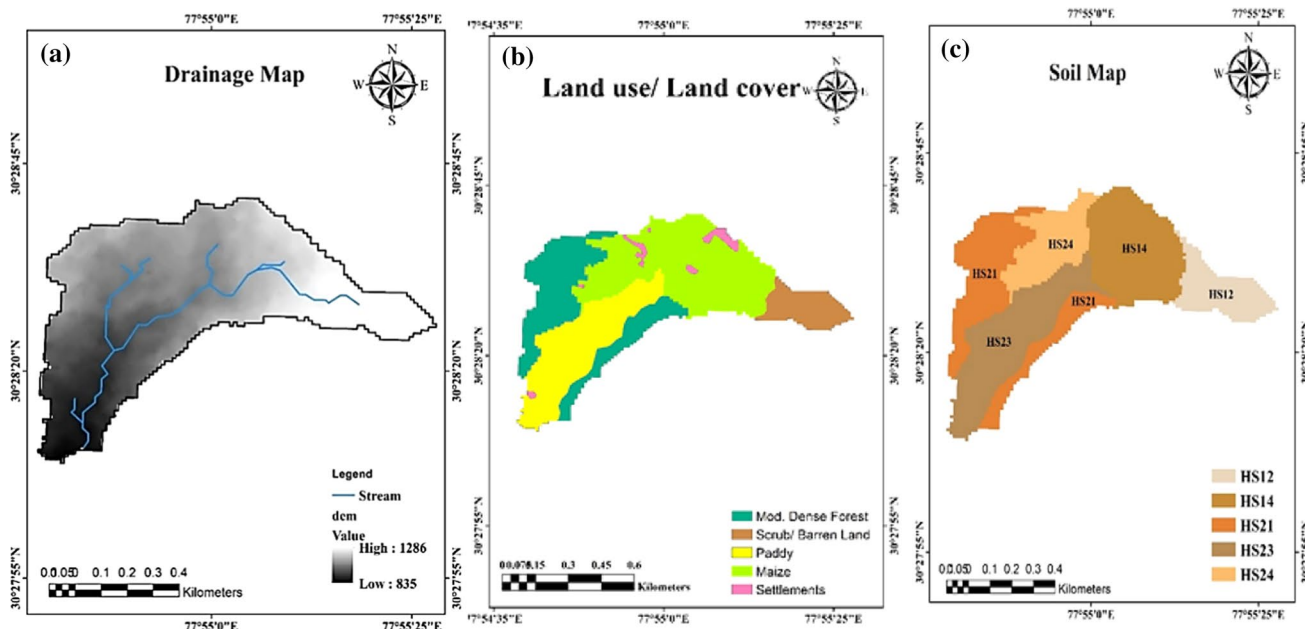


Fig. 5 Elevation with drainage (a), land use/land cover map (b), soil-landscape map (c)

Table 1 Soil physiographic unit classification

Geomorphology	Topography	Land use/land cover	Legend
Hillside slope (HS)	Very steep	Scrub land	HS12
		Crop land (Maize)	HS14
	Steep to very steep	Moderately dense forest	HS21
		Moderately steep	Crop land (Paddy)
		Crop land (Maize)	HS24

Physiographic soil units (Fig. 5c) were created based on the geomorphology, topography, and LULC. The topography of the study area is divided into three; very steep, steep to very steep, and moderately steep. Scrubland and maize cropping come under the very steep area. Steep to very steep category includes moderately dense forest while maize and paddy classified under moderate slope topography. This topography comes under the hillside slope (HS) (Table 1). Soils were characterised by dominantly sandy loam in texture with bulk density ranging from 1.12 to 1.56 g cm⁻³. Soil organic matter in the surface soil ranges from 1.2 (scrub land) to 4.2% (agricultural land). Unsaturated hydraulic conductivity ranges from 2.7 to 11.4 mm hr⁻¹ in the watershed. The surface and sub-surface's primary physical and chemical properties are grouped into the table (Table 2).

4.2 SWAT model simulation

4.2.1 Sensitivity analysis

Prior to calibration, sensitivity analysis was carried out to find the sensitive parameters of runoff and sediment yield. Sensitivity analysis revealed that runoff is sensitive to curve number (CN) and available water content (AWC) and sediment yield is sensitive to crop management factor (USLE-C) and crop practice factor (USLE-P). The results in the Table 3 shows that the surface runoff is more sensitive to the variations in the curve number. The percentage change in parameter value (change mentioned in Table 3) assigned from a previous study using SWAT model at Sitla Rao watershed (Singh, 2009) and considerable change in surface runoff and sediment yield were observed while adding and subtracting the parameters by the assigned values. Negligible change was observed for changing the lower values. Change in curve number by 4 and resulted in a variation of 57 and -32.8% in surface runoff. The second major sensitive parameter is Available Water Content exhibits -8.2%. Sediment yield is sensitive to USLE-C, USLE-P and BIOMIX. In these, USLE-P is the most sensitive parameter. 5 and -5 variation in USLE-P factor resulted in 81 and -98% change in sediment yield. BIOMIX was observed as the second major sensitive parameter of a value of -57.9. Kumar et al. (2016) also identified the sensitive parameters for the SWAT model for surface runoff. The present study results are also on par with that.

Table 2 Surface and sub-surface soil physicochemical properties

Legend	Clay (%)	Texture	pH	EC (dS/m)	Organic matter (%)	Coarse fragment (%)	Bulk density (g/cm ³)	Unsaturated hydraulic conductivity (mm/hr)
HS12	17	Sandy Loam	5.2	0.22	1.2	28	1.56	2.7
	14	Sandy Loam	5.3	0.18	1.1			
HS14	14	Sandy Loam	5.9	0.14	4.2	18	1.42	6.2
	15	Sandy Loam	4.5	0.13	3.8			
HS21	13	Sandy Loam	3.7	0.03	3.9	12	1.12	8.2
	14	Sandy Loam	3.7	0.03	3.0			
HS23	14	Loam	4.3	0.04	2.1	8	1.26	11.4
	13	Sandy Loam	4.7	0.04	1.7			
HS24	17	Loam	4.8	0.11	1.6	10	1.36	8.4
	17	Loam	5.0	0.14	1.4			

Table 3 Sensitivity analysis for the SWAT model parameters

Sl.no	Parameters	Change	Surface runoff (%)	Sediment yield (%)
1	Curve number (CN)	-4	-32.8	-30.76
		4	57	54.7
2	Available water content (AWC)	-0.05	-8.2	-2.4
		0.05	-1.9	-5.6
3	USLE-C	-25	1.10	-10.73
		25	1.09	11.4
4	USLE-P	-5	-45.1	-98
		5	45.4	81
5	Slope	-25	-1.13	-35.85
		25	1.12	40.9
6	BIOMIX	-50	-45	-57.9
		50	45.2	0.9

4.2.2 Surface runoff and sediment yield calibration

The model was calibrated manually for the surface runoff and sediment yield. Since the CN values and AWC are the highly sensitive factors for the runoff, thus changes were made in those values. The model predicted relatively well for low to medium rainfall events during the calibration. The model calibration (Fig. 6a) was assessed using the (r) of 0.94, the determination coefficient (r^2) of 0.89, PBIAS of -25.2 and RMSE of 4.67 mm/day, which means the calibrated model can explain 89% of the variation in the observed runoff. The low RMSE value indicates that the surface runoff predictions are satisfactory. The Box and Whisker plot (Fig. 6b) gives the distribution of observed and predicted surface runoff. According to PBIAS, the model is over predicting the surface runoff. PBIAS has an ideal value of 0.0, and low magnitude values indicate accurate model simulation. Positive values indicate underestimation bias in the model, whereas negative values suggest overestimation bias in the model (Gupta et al., 1999). The adjustment of USLE—P, USLE—C, and USLE—K factors were made for

sediment yield prediction and obtained satisfactory result. The model predicted relatively well for low to medium rainfall events during the sediment yield calibration. The model calibration (Fig. 6c) was assessed using the (r) of 0.94, a determination coefficient (r^2) of 0.89, PBIAS of 10.5, and RMSE of 0.055 t/ha/day, which means 89% of variation can be explained by the calibrated model (Table 4). The Box and Whisker plot (Fig. 6d) gives the distribution of the observed and predicted values. According to PBIAS, the model is slightly under predicting the sediment yield. It may be due to landslips in the watershed, which the SWAT model could not account for.

4.2.3 Surface runoff and sediment yield validation

After repeated adjustment of sensitive parameters, the most appropriate values of the sensitive parameters for surface runoff and sediment yield prediction were identified (Table 5). Then the model was validated for both runoff and sediment yield. From 28 daily runoff data, 12 days were used for validation. The model predicted relatively well for

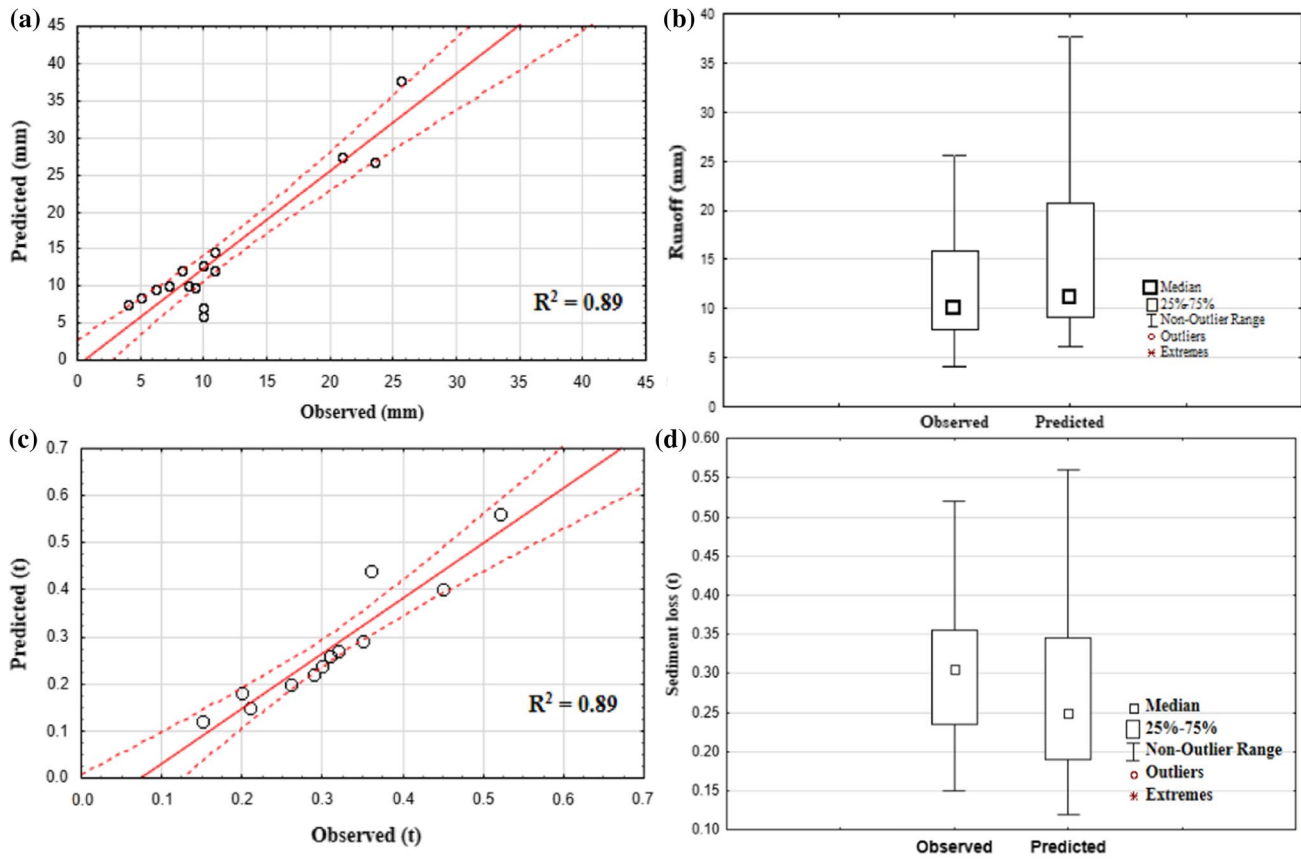


Fig. 6 Calibration regression plot and Box plot of observed and predicted surface runoff (a and b); Calibration regression plot and Box plot of observed and predicted sediment yield (c and d)

Table 4 Calibration statistics for surface runoff and sediment yield calibration

Statistical parameter	Surface runoff (mm)		Sediment yield (t/ha)	
	Observed	Predicted	Observed	Predicted
Total number (N)	16	16	12	12
Mean	11.978	14.996	0.310	0.277
Standard deviation	6.805	9.410	0.103	0.128
Maximum	25.64	37.72	0.520	0.580
Minimum	4.00	6.04	0.150	0.120
RMSE	4.673		0.055	
<i>r</i>	0.947		0.944	
<i>r</i> ²	0.89		0.89	
PBIAS	-25.2		10.5	

Table 5 Calibrated SWAT model parameters for surface runoff and sediment loss

Parameters for surface runoff	Prescribed range	Calibrated value
SCS Curve Number (CN)	35–98	Agriculture-80 Forest-72 Scrub-84
Available water content (AWC)	0–1	0.089–0.093
USLE-P	0–1	0.3–0.9
USLE-C	0.001–1	0.001–0.2
USLE-K	0–0.65	0.08–0.09

low to medium rainfall events during validation. For runoff, the model validation (Fig. 7a) was assessed using the (*r*) of 0.92, determination coefficient (*r*²) of 0.85, PBIAS of -10.1 and root mean square error (RMSE) of 2.79 mm/day, which means the calibrated model can explain 85% of the variation in the observed runoff (Table 6). The NSE value obtained for surface runoff is 0.81. Moriasi et al. (2007)

suggested that NSE estimates should surpass 0.5, then model results to be deemed satisfactory for the hydrologic process on a monthly time-step while relaxation applies to the daily time-step performance. The Box and Whisker plot (Fig. 7b) gives the distribution of observed and predicted surface runoff. According to the PBIAS, similar to the calibration, the model also slightly over predicts the surface runoff. Surface runoff over prediction was found for heavy rainfall events, which might be attributed to coarse fragments and stony surfaces in the watershed, but its impact was minor at low to

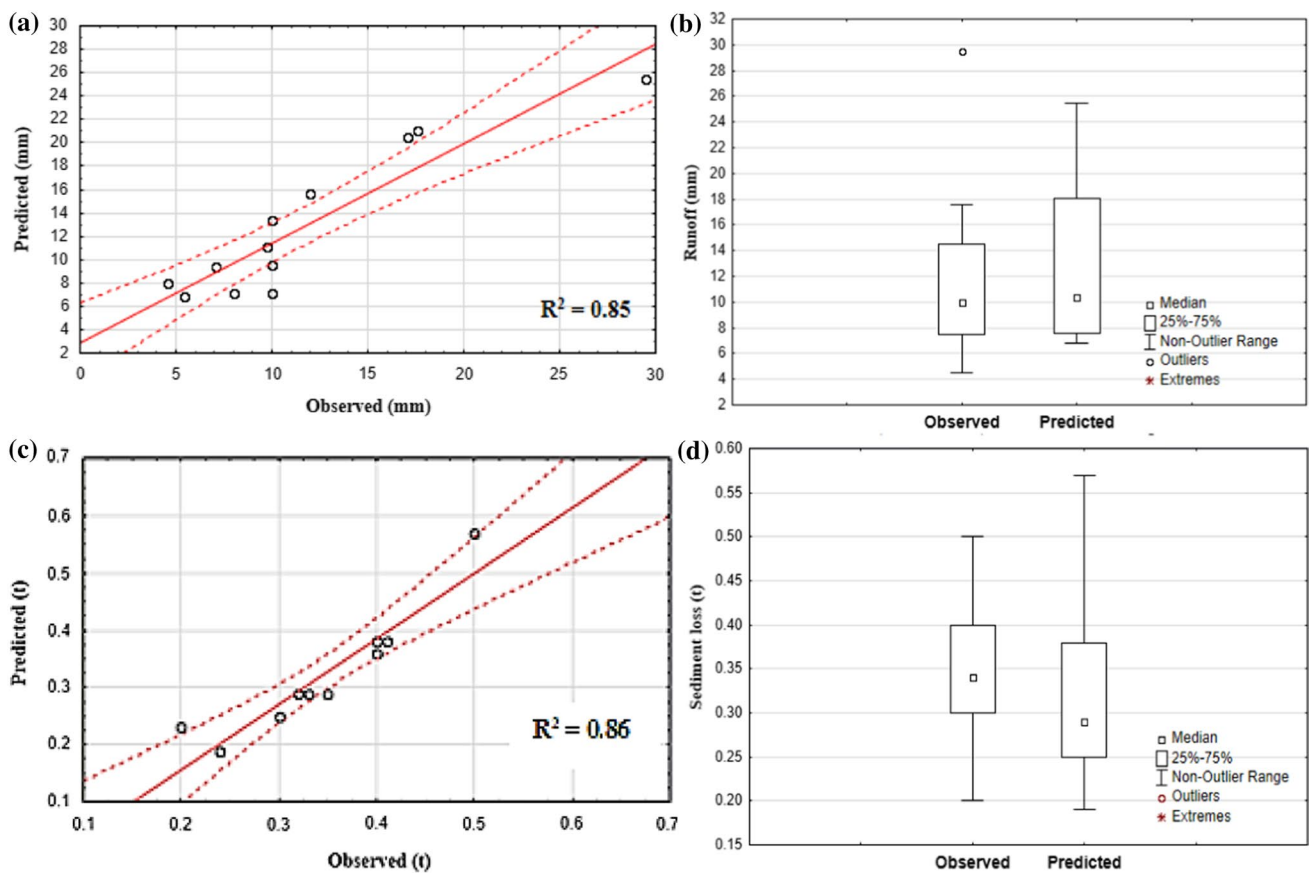


Fig. 7 Validation regression plot and Box plot of observed and predicted surface runoff (a and b); Calibration regression plot and Box plot of observed and predicted sediment yield (c and d)

Table 6 SWAT model validation performance

Parameters	Correlation coefficient (r)	Coefficient of determination (r^2)	Root mean square error (RMSE)	Nash–Sutcliffe model efficiency (NSE)	PBIAS
Surface runoff	0.92	0.85	2.79 mm/day	0.81	-10.1
Sediment yield	0.93	0.86	0.048 t /ha/day	0.70	6.4

medium rainfall events due to time lag and not accounted for by the model (Kumar et al., 2016, 2021; Park et al., 2017).

The model performance was good for low to medium rainfall events during the validation of sediment yield. The model validation (Fig. 7c) was assessed using a correlation coefficient (r) of 0.93, (r^2) of 0.86, PBIAS of 6.4 and RMSE of 0.048 t ha⁻¹ day⁻¹, which means 86% of variation can be explained by the calibrated model (Table 6). The lower RMSE value depicts that the validation processes are satisfactory. Figure 7d, the Box and Whisker plot gives the distribution of the observed and predicted sediment yield values. According to the PBIAS, the model is slightly under predicting. After the calibration and validation, the model performance for the sediment yield was assessed with the help of the NSE (0.70). Moriasi et al. (2007) suggested

that NSE estimates should surpass 0.5, then model results to be considered satisfactory for hydrologic processes on a monthly time step while relaxation applies to the daily time-step performance.

The PBIAS of $\pm 25\%$ for surface runoff and PBIAS of $\pm 55\%$ for sediment prediction is considered satisfactory in general for model simulation. PBIAS has the ability to clearly show when a model is not presenting a very accurate result (Gupta et al., 1999). The model performed exceptionally well for low to medium rainfall during simulation. However, the high rainfall events model overestimated the runoff and under predicted the sediment yield. Overestimated runoff may be due to the high surface coarse fragment and stoniness, contributing to the surface runoff (Singh, 2012). Qiu et al. (2012) also reported the under estimation of sediment

yield prediction by the SWAT model. Various other studies also reported the under and over estimation of surface runoff (Suliman et al., 2015). In addition to that, the cropland has the conservation practices like small stone bunds and terraces to reduce runoff, which cannot account by the model. Underestimation of sediment yield may be due to landslips/collapse of field terraces in Himalayan Region (Kumar et al., 2021). The minimum vegetation cover (during the fallow period) of the paddy field during monsoon (Singh, 2009) can also contribute to a higher sediment yield at the watershed outlet. Similarly, a study conducted in Sind River Basin, India using SWAT model results indicated that R^2 and NS were 0.77 and 0.74, respectively, during the calibration. The validation also indicated a satisfactory performance with R^2 of 0.71 and NS of 0.69 (Narsimlu et al., 2015). Also, a study carried out in Tons River Basin, the R^2 , NSE, and PBIAS were 0.74, 0.73, and -3.55 , respectively, during the calibration, whereas in validation period values were 0.75, 0.69, and 18.55, respectively (Kumar et al., 2017). The literature also provides the capability of SWAT model to simulate erosion processes reliably.

4.2.4 Surface runoff and soil loss prediction

After the calibration and validation, the SWAT model was run to predict surface runoff and soil loss from each HRU on a yearly scale. 13 HRUs were created by SWAT model based on the dominant LULC, soil, and slope. Predicting the runoff from different land uses, a high average annual runoff was generated from scrubland (930.53 mm/year) followed by paddy (720.87 mm/year), and then by maize (709.2 mm/year), while less runoff was predicted from the moderately dense forest (678.3 mm/year). Average surface runoff from various land uses shows that runoff from scrubland is higher due to less cover and the absence of conservation practices. Paddy and maize fields have conservation practices, although the breakage of bunds and terraces in the watershed during high-intensity rainfall causes the relatively high surface runoff. Since the moderately dense forest has more canopy and thus the rainfall interception energy was dissipated, low surface runoff was observed. The gradient, plant cover density, and stone cover of cut slopes exhibited statistically significant effects on runoff and erosion, according to Arnaez et al. (2004). Also, soil hydraulic conductivity was higher in forests than in pastures (Chandler et al., 2018). Thus, forest can reduce the surface runoff and associated sediment yield than the other land uses.

Similarly, predicted soil loss was also high in scrub land and low in moderately dense forest. Soil loss from paddy fields was observed as low, and runoff was high in the maize fields because of the overflow of standing water from the field. The highest soil loss was observed (Table 7; Fig. 8) from the HRU number 6, which is mainly occupied

Table 7 Soil loss from various HRUs

HRU	Dominant land use	Soil loss (t ha ⁻¹ year ⁻¹)
1	Maize	33.29
2	Moderately dense forest	21.39
3	Maize	29.53
4	Maize	31.36
5	Maize	25.88
6	Scrub land	42.78
7	Moderately dense forest	19.49
8	Maize	31.07
9	Moderately dense forest	19.54
10	Paddy	24.00
11	Paddy	29.09
12	Paddy	24.19
13	Paddy	18.96

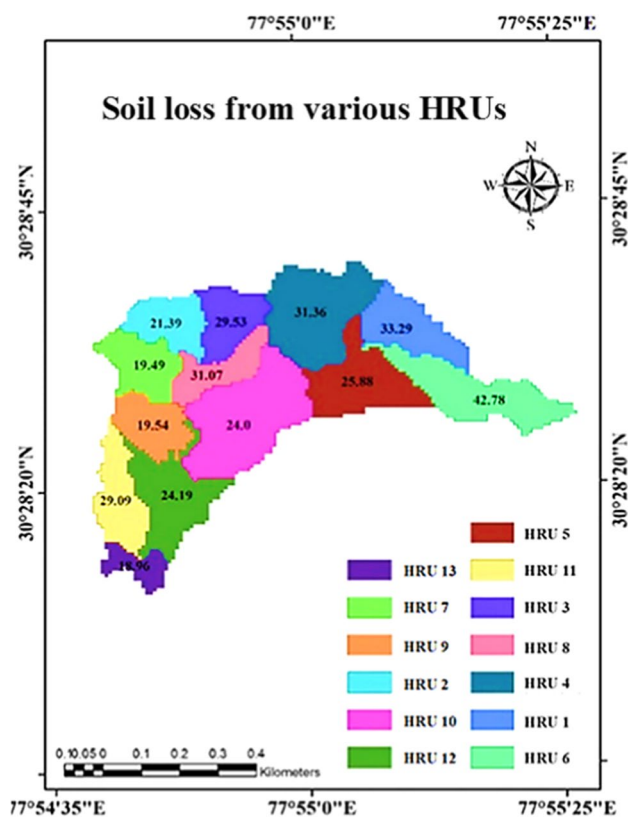


Fig. 8 Spatial distribution of soil loss (t ha⁻¹ year⁻¹) from various HRUs

by scrub land (42.78 t ha⁻¹ year⁻¹). Liu et al. (2020) also reported that scrubland had a greater runoff reduction effect than grassland and forest. The higher slope, less cover, and higher erodibility of the soils in the scrub land is the primary reason for higher soil erosion. HRU number 1, the

maize field at the upper part of the watershed, has a soil loss of $33.29 \text{ t ha}^{-1} \text{ year}^{-1}$, followed by HRU 4 and HRU 8 (maize) (Fig. 9a). Soil loss from HRU 13 observed as lowest ($18.9 \text{ t ha}^{-1} \text{ year}^{-1}$) among all. It is mainly because of the conservation measures (stone patch riser terrace; Fig. 9b) adopted in the paddy field. Forest in the watershed is moderately dense, and these are under the threat of erosion. Soil loss of $19.49 \text{ t ha}^{-1} \text{ year}^{-1}$ from HRU 7, $19.59 \text{ t ha}^{-1} \text{ year}^{-1}$ from HRU 9, and $21.39 \text{ t ha}^{-1} \text{ year}^{-1}$ from HRU 2 were observed. The upper part (higher elevation and slope) of the watershed found to be more prone to erosion. While moderately dense Sal forest (Fig. 9c) and stone patching on riser of terraced paddy field showed relatively less prone to erosion. Soil loss from paddy fields was observed as low and runoff as high when compared to the maize fields because of the overflow of standing water from the field. The standing water also act as cover and protect soil from further detachment (Fig. 9d). Vegetation has been found to minimise runoff through canopy interception, increased soil permeability, root consumption for plant growth, and evapotranspiration in general (Gyssels & Poesen, 2003; de Baets et al., 2007). Furthermore, several studies have shown that increasing above-ground plant parts, litter layers, canopy and ground cover, and the soil binding effects supplied by

root systems minimises soil erosion. (Borrelli et al., 2017; Zhao et al., 2014).

Among different land uses (Fig. 10), significantly less average soil loss ($20.14 \text{ t ha}^{-1} \text{ year}^{-1}$) was observed in the moderately dense forest, followed by the paddy ($24.06 \text{ t ha}^{-1} \text{ year}^{-1}$). Higher soil erosion rates were observed in the scrub land ($42.78 \text{ t ha}^{-1} \text{ year}^{-1}$) and followed by the maize cropland ($30.2 \text{ t ha}^{-1} \text{ year}^{-1}$). The lower erosion rate in the moderately dense forest is mainly due to the forest cover, reducing the rainfall's impact directly to the soil. Less cover and higher slope lead to higher soil erosion rates in scrub land. Farmers are adopting conservation practices like stone patching on riser of terraces, bench terraces, stone bunds, etc., which helps to reduce soil erosion in the paddy field. The terraces field in the watershed, according to Kumar et al. (2021) and Yin et al. (2009), promotes rainfall to infiltrate into the soil, which helps to reduce surface runoff. Natural forest cover also helped to reduce surface runoff through canopy interception, increased water use, and surface roughness effects.

Singh (2012) carried out a previous study at the same watershed, Sitla Rao shows an average soil erosion of $24.66 \text{ t ha}^{-1} \text{ year}^{-1}$. However, the average soil erosion rate increased to $29.30 \text{ t ha}^{-1} \text{ year}^{-1}$ in the current period.

Fig. 9 Maize field (a), Stone patching on riser of terraces (b), Sal forest (c), and Standing water in the paddy fields during monsoon (d)

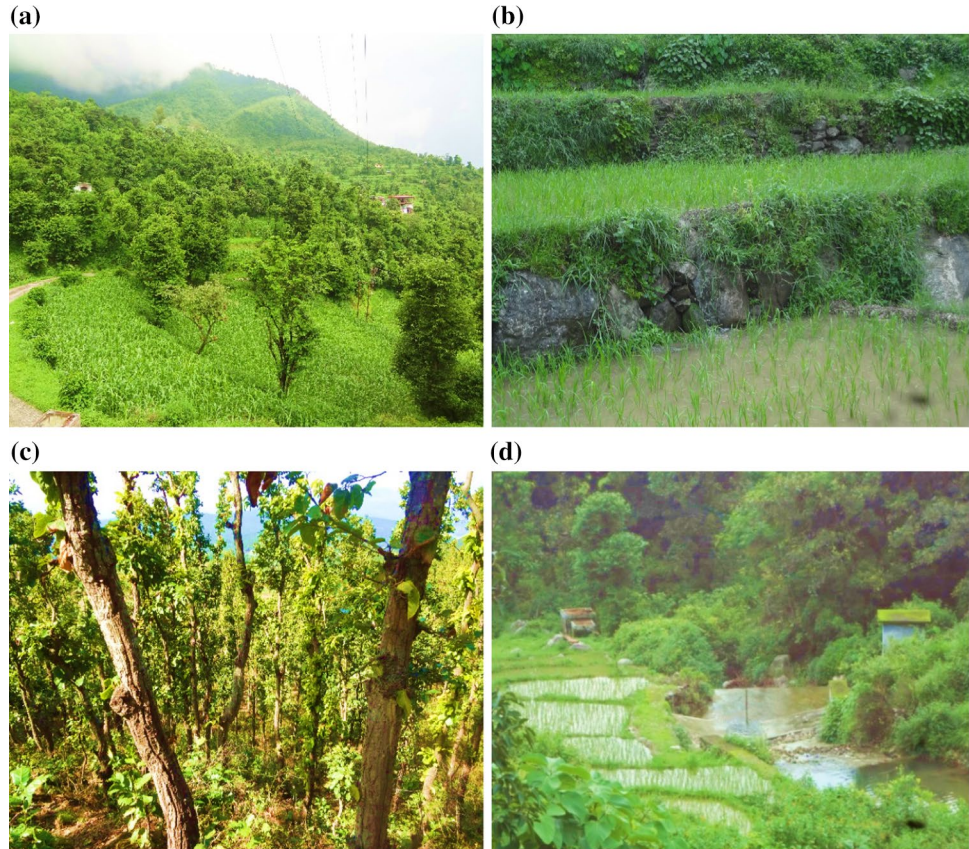
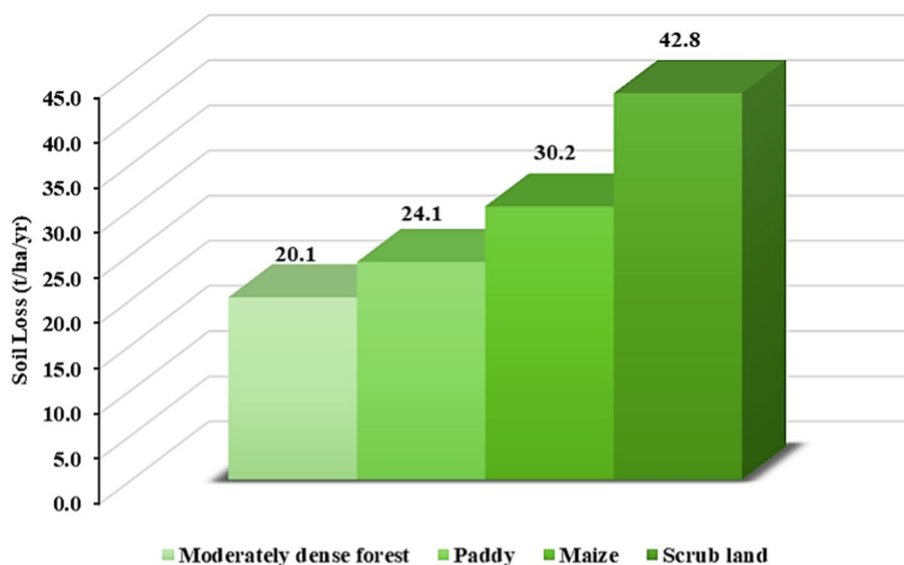


Fig. 10 Average soil loss from various land use/land cover



The Sitla Rao watershed produced average daily sediment in the range of 1.0–1.32 t ha⁻¹ with a peak of 3.04 t ha⁻¹ on a daily time-step, and average daily runoff 19.58 mm with a peak of 41 mm during the validation period (Kumar et al., 2021). Morgan et al. (1986) found that, in mountainous places, soil loss up to 25 t ha⁻¹ year⁻¹ is considered tolerable. In this study, it is quite higher than the tolerable limit. The majority of the subarea soil erosion is above 25 t ha⁻¹ year⁻¹. A study carried out at Pathri Rao sub-watershed in the Himalayan Shivalik area, Kumar and Kushwaha (2013) predicted an average annual soil erosion rate of 35.47 t ha⁻¹ year⁻¹ using RUSLE. According to Mandal et al. (2010), in the north-western Himalayas, the standard soil loss tolerance limit (SLTL) ranges from 2.5 to 12.5 t ha⁻¹ year⁻¹ and is followed for planning soil conservation activities. It is evident that most of the HRUs have soil erosion levels higher than 20 t ha⁻¹ year⁻¹, which is a matter of grave concern from the point of view of conservation of natural resources and agricultural production.

4.3 Projected future rainfall scenario

MarkSim DSSAT weather generator tool was used to obtain a downscaled future climate scenario to understand future rainfall changes. As per the IPCC recommendation, an average of the models available in MarkSim was downloaded and analysed the rainfall parameter under both the RCPs of 4.5 and 8.5 from 2011 to 2095. The rainfall changes under different scenarios discussed below.

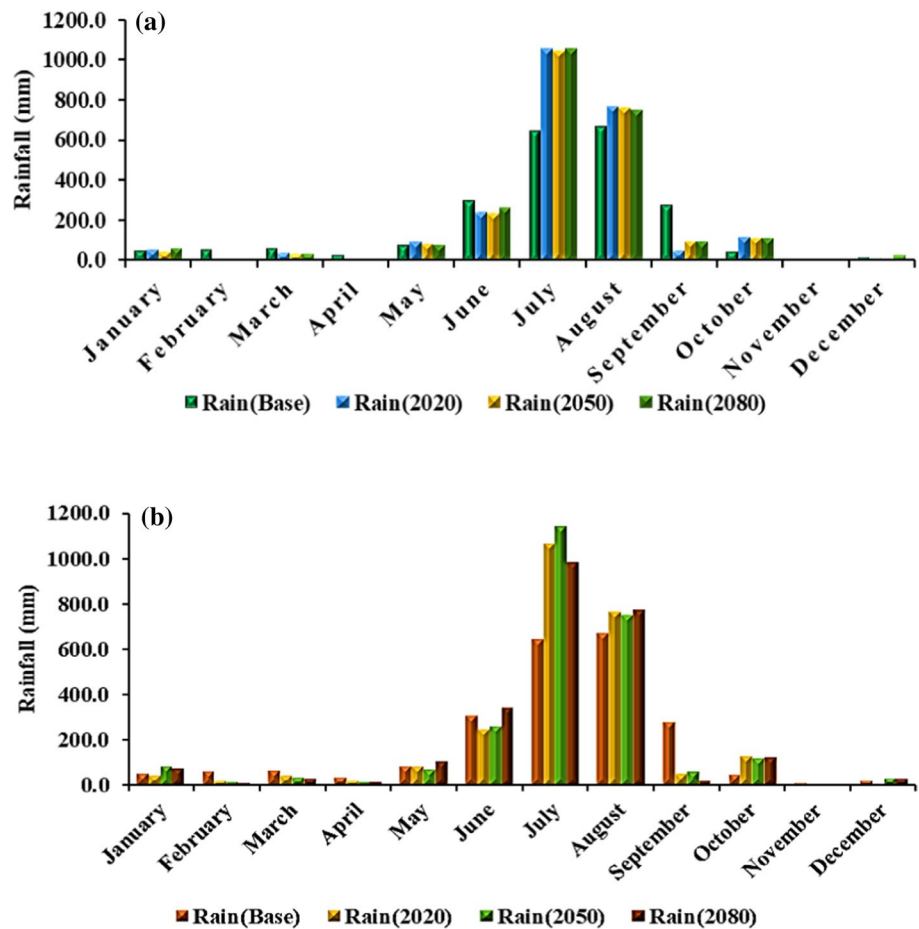
4.3.1 RCP 4.5 scenario

The climatic parameters were analysed with the baseline period (1986–2015) to study future changes in rainfall for the years; the 2020s (2011–2040), 2050s (2041–2070), and 2080s (2071–2095). These periods were represented as first, second, and third tricennial. It was observed that the average annual rainfall (Fig. 11a) of the study area is increasing under the RCP 4.5 scenario. The rainfall during the June and September months showed a decrease in the future period while July and August months showed a drastic increase. It indicated that during July and August, the intensity of rainfall may also increase. This increase in rainfall may lead to extreme soil erosion from the agricultural land because the rainy season crops are sowing in July, and there will be less protection for the soil during these periods. The average annual rainfall in the base period (1986–2015) is 2245.10 mm, while it is 2481.0 mm, 2469.4 mm, and 2521.8 mm, estimated for the three 30-year periods referred above. Kumar et al. (2015) conducted a study over six locations which are part of the Himalayan region. The results indicate a very significant positive trend in annual rainfall (22 mm/year) in these regions.

4.3.2 RCP 8.5 scenario

Under RCP 8.5, the average annual rainfall (Fig. 11b) shows an increase within the study area. The change in rainfall under this scenario is relatively greater than that under the RCP 4.5 scenario. The annual rainfall averages 2245.1 mm in the base period; however, it increased to 2440.4 mm in

Fig. 11 Change in monthly average rainfall from baseline under RCP 4.5 (a) and RCP 8.5 scenario (b)



the first tricennial, 2564.3 mm in the second tricennial, and 2472.3 mm in the third tricennial. Similarly, in the intermediate scenario, the high emission scenarios also showed a higher rainfall in July and August, while June and September showed a decreasing trend. Under RCP 4.5, July month in 2080 has the highest amount of rainfall (1053.4 mm). While under the RCP 8.5 scenario, July month of 2050 has the highest rainfall (1140.7 mm). Similar to the RCP 4.5 scenario, this scenario also increases in rainfall during the July month contribute to higher soil erosion from crop land (Paddy and Maize).

Gupta and Kumar (2017) carried out a study at mid-Himalayas and exposed that average annual rainfall may increase by 23.79–33.3% for H3A2 and 27.87–31.67% H3B2 scenario during 2011–2099, while in the current study, rainfall increases by 10.5%, 9.9%, and 12.3% during first tricennial, second tricennial, and third tricennial, respectively, based on the RCP 4.5 scenario. By the 2050s, rainfall will decrease slightly and increase by 12.3% during 2080s. The amount of rainfall based on the RCP 8.5 scenario from the base period showed an increase of 8.7%, 14.2%, and 10.1% in the first tricennial, second tricennial, and third tricennial. The 30-year average of projected rainfall indicates slight

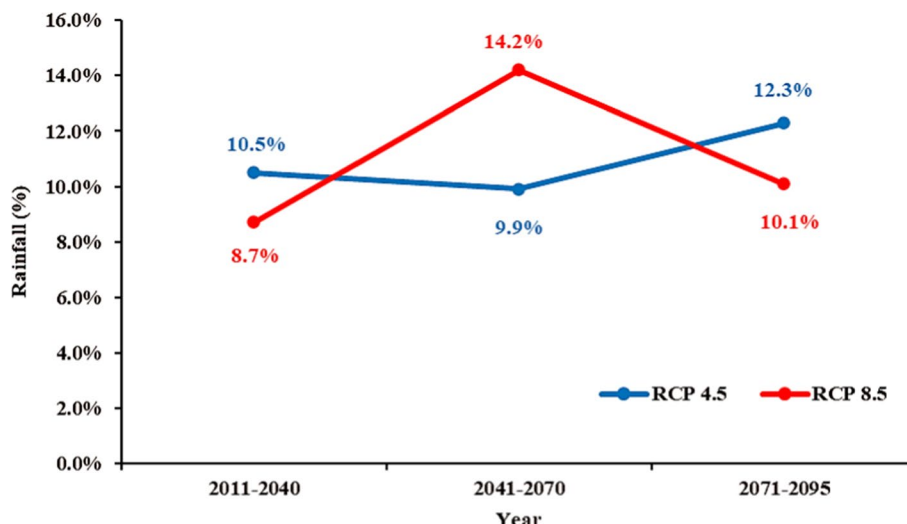
variations in both RCP8.5 and RCP 4.5 during the second tricennial (Fig. 12).

Under the RCP 8.5 scenario, the highest and lowest changes in rainfall were seen in the 2050s (14.2%) and 2020s (8.7%). Rainfall is anticipated to increase throughout all states, with the western part of the country experiencing the slightest change and the northern, eastern, and southern regions experiencing the most change under RCP 8.5. Based on the RCP 8.5, the country experiences an overall increase in Arunachal Pradesh and Haryana (Yaduvanshi et al., 2019). These rainfall estimations suggest the necessity for changes in agricultural management methods such as early soil preparation and sowing activities. The change in rainfall pattern may worsen the nation's food production, particularly in a country with rain fed agriculture is prominent.

4.4 Future soil loss

Similar to the future rainfall scenario, future soil loss also showed an increasing trend under both RCP scenarios. The average soil loss from different land uses were estimated based on RCPs for the first tricennial, second tricennial, and

Fig. 12 Percentage change in rainfall under RCP 4.5 and RCP 8.5



third tricennial. Percentage change of soil loss with the baseline period was also identified.

4.4.1 Future soil loss under RCP 4.5 scenario

Future climate scenario analysis showed that the periods of first tricennial, second tricennial, and third tricennial rainfall is expected to increase 10.5%, 9.9%, and 12.3%, respectively, from the baseline under RCP 4.5. The average soil loss under the RCP 4.5 (Table 8) scenario increased up to 18.1% from the baseline during 2080, 15.5% during 2020, and 14.6% during the 2050s. This result showed that the highest expected change in rainfall in the 2080s (12.3%) has the highest soil loss. Soil erosion was examined across a variety of land uses/covers, and the highest rate of erosion was discovered in scrublands (42.78–53.20 t ha⁻¹ year⁻¹), followed by agricultural fields (Maize) (30.23–36.07 t ha⁻¹ year⁻¹), and followed by paddy (24.06–28.22 t ha⁻¹ year⁻¹). However, in the RCP 4.5 scenario, the mod. dense forest was found to have less erosion risk (20.14 to 22.43 t ha⁻¹ year⁻¹). At the same time, the average soil erosion increases from 29.3 to 35 t ha⁻¹ year⁻¹ based on RCP 4.5, with a percentage change of 18.1 during the twenty-first century. Zheng et al. (2007) estimated that a 4–18% increase in rainfall could cause a 49–112% increase in runoff and a 31–167% surge

in soil loss. Akarsh (2013) conducted a study showing that soil erosion increases from 37.97 to 221.99% under the A2a scenario from 2020 to 2080, from the base period over the Doon valley, Uttarakhand. Less erosion rate was observed in the moderately dense forest due to cover factor and the higher erosion rate observed in scrub land due to the absence of cover and management practices. Pal and Chakraborty (2019) reported a higher rate of soil erosion under the RCP 6 and 8.5 while comparably less soil erosion under RCP 2.6 and 4.5. Narsimlu et al. (2013) reported that increase in surface runoff was estimated using SWAT model due to the increased rainfall projected from IPCC A1B scenario.

4.4.2 Future soil loss under RCP 8.5 scenario

Under this scenario, expected rainfall for the period 2020s, 2050s, and 2080s increased 8.7%, 14.2%, and 10.1%, respectively, from the baseline. The RCP 8.5 (Table 9) represents a higher emission scenario and shows higher rainfall changes resulting in a higher average soil erosion rate during the 2050s of 20.9% and less soil erosion during the 2020s (12.8%). RCP 8.5 scenario predicts relatively higher rainfall than RCP 4.5, so erosion was low in the RCP 4.5 scenario. Soil erosion was examined across a variety of land uses/covers, and the highest rate of erosion was discovered

Table 8 Average annual soil loss (t ha⁻¹ year⁻¹) and the change in percentage from different land use under 4.5 scenario

Land Use	Average soil loss (t ha ⁻¹ year ⁻¹)				Change in soil loss (%)		
	Present	2020s	2050s	2080s	2020s	2050s	2080s
Maize	30.23	35.25	34.94	36.07	16.61	15.57	19.33
Mod. dense forest	20.14	22.10	21.99	22.43	9.73	9.18	11.39
Scrubland	42.78	51.67	51.15	53.20	20.77	19.56	24.36
Paddy	24.06	27.61	27.41	28.22	14.75	13.91	17.28
Average	29.3	34.2	33.9	35.0	15.5	14.6	18.1

Table 9 Average annual soil loss ($\text{t ha}^{-1} \text{ year}^{-1}$) and the change in percentage from different land use under 8.5 scenario

Land use	Average soil loss ($\text{t ha}^{-1} \text{ year}^{-1}$)				Change in soil loss (%)		
	Present	2020s	2050s	2080s	2020s	2050s	2080s
Maize	30.23	34.37	36.98	35.03	13.69	22.32	15.88
Mod. dense forest	20.14	21.77	22.79	22.03	8.07	13.14	9.36
Scrubland	42.78	50.15	54.90	51.43	17.23	28.33	20.21
Paddy	24.06	26.99	28.86	27.48	12.20	19.94	14.19
Average	29.3	33.3	35.9	34.0	12.8	20.9	14.9

in scrublands ($42.78\text{--}54.90 \text{ t ha}^{-1} \text{ year}^{-1}$) and followed by agricultural fields (Maize) ($30.23\text{--}36.98 \text{ t ha}^{-1} \text{ year}^{-1}$), followed by paddy ($24.06\text{--}28.86 \text{ t ha}^{-1} \text{ year}^{-1}$). However, in the RCP 8.5 scenario, the moderately dense forest was found to have less erosion risk ($20.14\text{--}22.79 \text{ t ha}^{-1} \text{ year}^{-1}$). Under the RCP 8.5 scenario, soil erosion increases to 12.8% and further increases to 21% and further reduced to 15% during the first tricennial, second tricennial, and third tricennial, respectively. This increase may lead to soil degradation from the agricultural field. Which further reduces the soil quality, health as well as natural resistance of soil. This can lead to use decreased agricultural productivity from the high land agriculture. Policy makers and planners must pay special attention to the impacted areas to reduce the quantity of soil loss. To avoid a situation like this, structural and non-structural precautions must be adopted. Local governments and others have previously taken steps to mitigate top soil loss. However, given the circumstances, such approaches may not be appropriate to address the problem and may violate sustainable land management norms (Chakraborty et al., 2020). As a result of the findings, forests may be able to withstand future surface soil erosion, and social forestry with exterior plant species may be able to alleviate the problem of increased erosion in agricultural fields. Soil erosion can be reduced to a greater extent in agroforestry-style agricultural fields.

Similarly, the average annual soil erosion rate over the Mahi River basin increased by 11.2% based on the ensemble means of the climate model (Maurya et al., 2021). In contrast, the average soil erosion increases from 29.3 to 35.9 $\text{t ha}^{-1} \text{ year}^{-1}$ based on RCP 8.5 with a percentage change of 21 during the twenty-first century. Gupta and Kumar (2017) carried out a study at mid-Himalayan landscape and unveiled that the average annual soil erosion rate may increase by 28.38%, 25.64%, and 20.33% under the H3A2 emission scenario during the first tricennial, second tricennial, and third tricennial. Owing to changes in rainfall intensity and volume, the erosive potential of soil particles rises, whereas future average global soil erosion is expected to increase by 9% due to climate change by 2090 (Yang et al., 2003). From the 2020s through the 2080s, there is a progressive increase in the rate of soil erosion. Using support vector machine (SVM) downscaled data, soil loss increased up

to $4.75 \text{ t ha}^{-1} \text{ year}^{-1}$ from the 2020s to the 2080s, while the statistical downscaling models (SDSM) model predicts an increase up to $6.10 \text{ t ha}^{-1} \text{ year}^{-1}$ from the 2020s to the 2080s (Mondal et al., 2015). A study conducted in Eastern India, Chakraborty et al. (2020) revealed that severe precipitation rates with high kinetic energy due to climate change are favourable to soil erosion susceptibility. Pal et al. (2021) also indicated that soil erosion will become more prevalent in the future (2040, 2060, 2080, and 2100s). So, in sub-tropical monsoon-dominated nations like India, the potential impact of climate change on soil erosion has been established. Under the representative concentration pathway (RCP) 4.5 and RCP 8.5 emission scenarios, Rajbanshi and Bhattacharya (2021) calculated that a 3.67–11.08% increase in rainfall-runoff erosivity and might result in a 3.7–11.76% increase in soil erosion and sediment production in the watershed.

The increase in rainfall due to climate change is observing several regions around the world. The sloppy terrain with high-intensity rainfall may exacerbate the soil erosion in the hilly and mountainous region. Several researchers stated the increase in soil erosion due to climate change around different regions Brazil (Anache et al., 2018), Iran (Doulabian et al., 2021), Pakistan (Ashraf, 2020), Thailand (Sirikaew et al., 2020), and Morocco (Simonneaux et al., 2015). Although, the soil erosion decrease due to rainfall was also observed by Stefanidis and Stathis (2018) over Greece. Similarly, in India, several studies reported the impact of climate change on soil erosion over West Bengal (Pal & Chakraborty, 2019), Western India (Maurya et al., 2021), Uttarakhand (Khare et al., 2017), Narmada River basin (Mondal et al., 2016). While comparing the soil erosion percentage change with other studies is often complex, because the change in erosion rate may differ according to a regions' topography, soil type, land use/land cover, and management practices adopted. Thus, the change in soil erosion with different rainfall scenario also may vary based on the site characteristics.

As additional increases in soil erosion are anticipated in catchments due to climate change, vegetative and structural control measures are urgently required to mitigate the threat of soil erosion. In a mildly sloping area (1–6%) contour farming is helpful to reduce energy of runoff water. Tillage

makes soil surface more permeable to infiltration of rainwater. This practice also reduces runoff, soil and nutrient losses and enhance crop yield. Mechanical measures like contour bunds can be used for soil conservation. To reduce the slope and slope length bench terrace can be used. Maintenance and strengthening of terraces and stone bunds in the cropland by growing grass along the bund and terraces can reduce the chances of breakage of these and overflow of runoff water during monsoon season. For suitable natural drainage grassed waterways are essential on agricultural land. Since the watershed belongs to the Doon valley it is suitable to use different grasses like *Panicum repens*, *Brachiaria mutica*, and *Cynodon plectostachyus*. For forest and scrubland trenching is helpful to reduce runoff and soil erosion. Hence, we suggest integrated multidimensional conservation measures to combat soil erosion due to climate change.

5 Conclusion

The soil erosion in the Himalayan region is very severe due to the sloping terrain and high-intensity rainfall. The future climate change may worsen this scenario than the current period. In this study, the MarkSim weather generator tool was used to obtain the downscaled future climatic variable (Rainfall) at a point scale. The average rainfall of the baseline period (1986–2015) was estimated as 2245.1 mm. Analysis of rainfall based on RCP 4.5 and 8.5 exhibited an increasing trend in the future from the baseline period. Under the RCP 4.5 and 8.5 pathways, rainfall is anticipated to increase from 12.3 to 14.2%. The calibrated SWAT model was performed exceptionally well for low to medium rainfall but overestimated surface runoff and underestimated the sediment yield. The r^2 , PBIAS and RMSE of runoff validation were 0.85, -10.1 , and 2.79 mm, respectively. For sediment yield validation, r^2 was 0.86, PBIAS was 6.4, and RMSE was 0.048 t ha⁻¹. Also, the Nash-Sutcliffe Efficiency for the surface runoff was 0.81 and sediment yield was 0.70. Hence, the SWAT model was satisfactory with the applicability and performance in the humid subtropical Himalayan watershed. The highest soil loss occurred from scrubland (42.78 t ha⁻¹ year⁻¹), which belongs to the high slope areas and least cover, followed by maize (30.23 t ha⁻¹ yr⁻¹) and paddy (24.06 t ha⁻¹ year⁻¹). The fewer soil loss was predicted from the moderately dense forest (20.14). At present, the average annual soil loss from the watershed is 29.3 t ha⁻¹ year⁻¹, while under RCP 4.5, it is expected to increase up to 35 t ha⁻¹ year⁻¹ in the 2080s. Under RCP 8.5, soil loss is expected to increase up to 35.9 t ha⁻¹ year⁻¹ in the 2050s. Increased rainfall has resulted in a variation or an increase in future soil erosion. Compared to the current or observed time to a future period,

a significant increase in soil erosion was observed. Under RCP 4.5, the percentage change in soil loss in the 2080s and 2020s is higher than in the 2050s and enormous soil loss was predicted in the 2050s and 2080s under RCP 8.5. The study has a limitation; it only considered rainfall, indicating that more rainfall will increase soil erosion. Other characteristics, such as soil type, land use, and slope, were treated as constants in the future. Although the study confirms that the region's agricultural and scrub lands are more prone to erosion, owing to differences in tillage, conservation and cropping time. Moreover, climate change will pose a significant threat to soil erosion in the future.

Various climate models and emission pathways forecast varied amounts of rainfall, resulting in different climate projections. It is critical to emphasise that while the study does not provide precise soil erosion estimates, it provides scientists and policymakers with solid systematic evidence of future soil erosion in the humid subtropical Lesser Himalayas. Soil erosion by water is the major land degradation problem around the world. The mountainous terrain like Himalayas is prominent in present situation. To reduce the soil quality degradation due to intensive soil erosion needs proper conservation and land use planning in Himalayan region where high land agriculture is prominent. The study predicting increase rainfall depth during various scenarios. This further enhances the soil erosion from fragile Himalayan mountains. This can lead to decreased productivity from the high land agriculture. To offset this, planners need to implement the policies which can reduce the soil erosion from the agricultural land. Based on the erosion severity in various regions, they can adopt site-specific practices. These kinds of reliable scientific information provide efficient sustainable adaptation and mitigation measures for the decision makers. Thus, the future increase in soil erosion can be ameliorated with reforestation and afforestation, as the moderately dense forest cover showed less soil erosion in the future than the other land uses. It also revealed that integrated multidimensional soil conservation methods are critical in the watershed, mainly where the land is in a state with high soil erosion.

Acknowledgements Authors are thankful to the Director, Indian Institute of Remote Sensing (IIRS), for providing necessary facilities and other supports under the Earth Observation Applications Mission (EOAM) Project (ISRO/DOS) on “Mountain Ecosystem Processes and Services” to carry out the research work. Authors sincerely acknowledge Late Shri P. V. Rama Raju, IIRS, Dehradun and Sri R. K. Arya, Technical Officer, ICAR-IISWC, Dehradun for providing technical guidance in constructing and developing the watershed gauging site. Authors are also thankful to the Dean, College of Climate Change and Environmental Science (CCCES), Kerala Agricultural University.

Author contributions Conceptualization: KRS and SK; Methodology: KRS and ADR; Formal analysis, data collection, and investigation: KRS and ADR; Writing—original draft preparation: KRS;

Writing—review and editing: SK, MR, and ADR; Supervision: SK and MR. All authors read and approved the final manuscript.

Funding Not applicable.

Data availability The future climate datasets generated and analysed during the current study are available on the <http://gismap.ciat.cgiar.org/MarkSimGCM/> website. In addition, the satellite, soil, land use, surface runoff, and sediment data that support the findings of this study were obtained from the Indian Institute of Remote Sensing (IIRS), Indian Space Research Organization (ISRO), but restrictions apply to the availability of these data, which were used under licence for the current study, and so are not publicly available.

Declarations

Conflict of interest The authors declare that they have no known competing financial interests or personal relationships that could have appeared to influence the work reported in this paper.

References

- Aawar, T., & Khare, D. (2020). Assessment of climate change impacts on streamflow through hydrological model using SWAT model: A case study of Afghanistan. *Modeling Earth Systems and Environment*, 6(3), 1427–1437.
- Abbaspour, K. C., Rouholahnejad, E., Vaghefi, Srinivasan, R., Yang, H., & Kløve, B. (2015). A continental-scale hydrology and water quality model for Europe: Calibration and uncertainty of a high-resolution large-scale SWAT model. *Journal of Hydrology*, 524, 733–752.
- Akarsh, A. (2013). Surface runoff, Soil erosion and Water Quality estimation using APEX model integrated with GIS—A case study in Himalayan Watershed. M. Tech (RS& GIS) thesis, Andra University, Andra Pradesh, 80p.
- Alam, S., Ali, M., Rahaman, A. Z., & Islam, Z. (2021). Multi-model ensemble projection of mean and extreme streamflow of Brahmaputra River Basin under the impact of climate change. *Journal of Water and Climate Change*, 12, 2026–2044.
- Alewell, C., Borrelli, P., Meusburger, K., & Panagos, P. (2019). Using the USLE: Chances, challenges and limitations of soil erosion modelling. *The International Soil and Water Conservation Research*, 7, 203–225. <https://doi.org/10.1016/j.iswcr.2019.05.004>
- Anache, J. A., Flanagan, D. C., Srivastava, A., & Wendland, E. C. (2018). Land use and climate change impacts on runoff and soil erosion at the hillslope scale in the Brazilian Cerrado. *Science of the Total Environment*, 622, 140–151.
- Arnaez, J., Larrea, V., & Ortigosa, L. (2004). Surface runoff and soil erosion on unpaved forest roads from rainfall simulation tests in northeastern Spain. *CATENA*, 57(1), 1–14.
- Arnold, J. G., Moriasi, D. N., Gassman, P. W., Abbaspour, K. C., White, M. J., Srinivasan, R., et al. (2012). SWAT: Model use, calibration, and validation. *Transactions of the ASABE*, 55(4), 1491–1508.
- Arnold, J. G., Williams, J. R., & Maidment, D. R. (1995). Continuous-time water and sediment-routing model for large basins. *Journal of Hydraulic Engineering*, 121(2), 171–183.
- Ashraf, A. (2020). Risk modeling of soil erosion under different land use and rainfall conditions in Soan river basin, sub-Himalayan region and mitigation options. *Modeling Earth Systems and Environment*, 6(1), 417–428.
- Azari, M., Moradi, H. R., Saghafian, B., & Faramarzi, M. (2016). Climate change impacts on streamflow and sediment yield in the North of Iran. *Hydrological Sciences Journal*, 61(1), 123–133.
- Bagwan, W. A., & Gavali, R. S. (2021). Delineating changes in soil erosion risk zones using RUSLE model based on confusion matrix for the Urmodi river watershed, Maharashtra, India. *Modeling Earth Systems and Environment*, 7(3), 2113–2126.
- Balascio, C. C., Palmeri, D. J., & Gao, H. (1998). Use of a genetic algorithm and multi-objective programming for calibration of a hydrologic model. *Transactions of the ASAE*, 41(3), 615.
- Ballabio, C., Borrelli, P., Spinoni, J., Meusburger, K., Michaelides, S., Beguería, S., et al. (2017). Mapping monthly rainfall erosivity in Europe. *Science of the Total Environment*, 579, 1298–1315.
- Borrelli, P., Alewell, C., Alvarez, P., Anache, J. A. A., Baartman, J., Ballabio, C., et al. (2021). Soil erosion modelling: A global review and statistical analysis. *Science of the Total Environment*, 780, 146494.
- Borrelli, P., Robinson, D. A., Fleischer, L. R., Lugato, E., Ballabio, C., Alewell, C., et al. (2017). An assessment of the global impact of 21st century land use change on soil erosion. *Nature Communications*, 8(1), 1–13.
- Boufala, M. H., El Hmadi, A., Essahlaoui, A., Chadli, K., El Ouali, A., & Lahjouj, A. (2021). Assessment of the best management practices under a semi-arid basin using SWAT model (case of M'dez watershed Morocco). *Modeling Earth Systems and Environment*. <https://doi.org/10.1007/s40808-021-01123-6>
- Briak, H., Mrabet, R., Moussadek, R., & Aboumaria, K. (2019). Use of a calibrated SWAT model to evaluate the effects of agricultural BMPs on sediments of the Kalaya river basin (North of Morocco). *International Soil and Water Conservation Research*, 7(2), 176–183.
- Chakraborty, R., Pradhan, B., Mondal, P., & Pal, S. C. (2020). The use of RUSLE and GCMs to predict potential soil erosion associated with climate change in a monsoon-dominated region of eastern India. *Arabian Journal of Geosciences*, 13(20), 1–20.
- Chandler, K. R., Stevens, C. J., Binley, A., & Keith, A. M. (2018). Influence of tree species and forest land use on soil hydraulic conductivity and implications for surface runoff generation. *Geoderma*, 310, 120–127.
- David Raj, A., Kumar, S., Regina, M., Sooryamol, K. R., & Singh, A. K. (2021). Calibrating APEX model for predicting surface runoff and sediment loss in a watershed—a case study in Shivallik region of India. *International Journal of Hydrology Science and Technology*. <https://doi.org/10.1504/IJHST.2021.10041820> in Press.
- De Baets, S., Poesen, J., Knapen, A., Barberá, G. G., & Navarro, J. A. (2007). Root characteristics of representative Mediterranean plant species and their erosion-reducing potential during concentrated runoff. *Plant and Soil*, 294(1), 169–183.
- Doetterl, S., Van Oost, K., & Six, J. (2012). Towards constraining the magnitude of global agricultural sediment and soil organic carbon fluxes. *Earth Surface Processes and Landforms*, 37(6), 642–655.
- Doulabian, S., Toosi, A. S., Calbimonte, G. H., Tousi, E. G., & Alaghamand, S. (2021). Projected climate change impacts on soil erosion over Iran. *Journal of Hydrology*, 598, 126432.
- Ficklin, D. L., Luo, Y., Luedeling, E., & Zhang, M. (2009). Climate change sensitivity assessment of a highly agricultural watershed using SWAT. *Journal of Hydrology*, 374(1–2), 16–29.
- Ganasri, B. P., & Ramesh, H. (2016). Assessment of soil erosion by RUSLE model using remote sensing and GIS—A case study of Nethravathi Basin. *Geoscience Frontiers*, 7(6), 953–961.

- García-Ruiz, J. M., Beguería, S., Nadal-Romero, E., González-Hidalgo, J. C., Lana-Renault, N., & Sanjuán, Y. (2015). A meta-analysis of soil erosion rates across the world. *Geomorphology*, *239*, 160–173.
- Gassman, P. W., Reyes, M. R., Green, C. H., & Arnold, J. G. (2007). The soil and water assessment tool: Historical development, applications, and future research directions. *Transactions of the ASABE*, *50*(4), 1211–1250.
- George, K. J., Kumar, S., Hole, R. M. (2021) Geospatial modelling of soil erosion and risk assessment in Indian Himalayan region—A study of Uttarakhand state. *Environmental Advances* *4*, 100039. <https://doi.org/10.1016/j.envadv.2021.100039>
- GSP. Global Soil Partnership Endorses Guidelines on Sustainable Soil Management (2017) <http://www.fao.org/global-soil-partnership/resources/highlights/detail/en/c/416516/>.
- Gupta, A. K., Negi, M., Nandy, S., Alatalo, J. M., Singh, V., & Pandey, R. (2019). Assessing the vulnerability of socio-environmental systems to climate change along an altitude gradient in the Indian Himalayas. *Ecological Indicators*, *106*, 105512.
- Gupta, H. V., Sorooshian, S., & Yapo, P. O. (1999). Status of automatic calibration for hydrologic models: Comparison with multilevel expert calibration. *Journal of Hydrologic Engineering*, *4*(2), 135–143.
- Gupta, S., & Kumar, S. (2017). Simulating climate change impact on soil erosion using RUSLE model—A case study in a watershed of mid-Himalayan landscape. *Journal of Earth System Science*, *126*(3), 43.
- Gwapedza, D., Nyamela, N., Hughes, D. A., Slaughter, A. R., Mantel, S. K., & van der Waal, B. (2021). Prediction of sediment yield of the Inxu River catchment (South Africa) using the MUSLE. *International Soil and Water Conservation Research*, *9*(1), 37–48.
- Gyssels, G., & Poesen, J. (2003). The importance of plant root characteristics in controlling concentrated flow erosion rates. *Earth Surface Processes and Landforms The Journal of the British Geomorphological Research Group*, *28*(4), 371–384.
- Himanshu, S. K., Pandey, A., Yadav, B., & Gupta, A. (2019). Evaluation of best management practices for sediment and nutrient loss control using SWAT model. *Soil and Tillage Research*, *192*, 42–58.
- Hu, J., Ma, J., Nie, C., Xue, L., Zhang, Y., Ni, F., et al. (2020). Attribution Analysis of Runoff change in Min-tuo River Basin based on SWAT model simulations, china. *Scientific Reports*, *10*(1), 1–16.
- Islam, M. R., Jaafar, W. Z. W., Hin, L. S., Osman, N., & Karim, M. R. (2020). Development of an erosion model for Langat River Basin, Malaysia, adapting GIS and RS in RUSLE. *Applied Water Science*, *10*(7), 1–11.
- Jemai, S., Kallel, A., Agoubi, B., & Abida, H. (2021). Soil erosion estimation in Arid area by USLE model applying GIS and RS: Case of Oued El Hamma Catchment, South-Eastern Tunisia. *Journal of the Indian Society of Remote Sensing*. <https://doi.org/10.1007/s12524-021-01320-x>
- Jones, P. G., & Thornton, P. K. (2000). MarkSim: Software to generate daily weather data for Latin America and Africa. *Agronomy Journal*, *92*, 445–453.
- Jones, P. G., & Thornton, P. K. (2013). Generating downscaled weather data from a suite of climate models for agricultural modelling applications. *Agricultural Systems*, *114*, 1–5.
- Kebede, Y. S., Endalamaw, N. T., Sinshaw, B. G., & Atinkut, H. B. (2021). Modeling soil erosion using RUSLE and GIS at watershed level in the upper beles. *Ethiopia. Environmental Challenges*, *2*, 100009.
- Khare, D., Mondal, A., Kundu, S., & Mishra, P. K. (2017). Climate change impact on soil erosion in the Mandakini River Basin, North India. *Applied Water Science*, *7*(5), 2373–2383.
- Krause, P., Boyle, D. P., & Base, F. (2005). Comparison of different efficiency criteria for hydrological model assessment. *Advances in Geosciences*, *5*, 89–97.
- Kumar, P. V., Rao, V. U. M., Bhavani, O., Venkateswarlu, B., Prasad, R., & Singh, R. (2015). Climatic change and variability in mid-Himalayan region of India. *Mausam*, *66*(2), 167–180.
- Kumar, S., & Kushwaha, S. P. S. (2013). Modelling soil erosion risk based on RUSLE-3D using GIS in a Shivalik sub-watershed. *Journal of Earth System Science*, *122*(2), 389–398.
- Kumar, S., Singh, A., & Shrestha, D. P. (2016). Modelling spatially distributed surface runoff generation using SWAT-VSA: A case study in a watershed of the north-west Himalayan landscape. *Modeling Earth Systems and Environment*, *2*(4), 1–11.
- Kumar, N., Singh, S. K., Srivastava, P. K., & Narsimlu, B. (2017). SWAT Model calibration and uncertainty analysis for stream-flow prediction of the Tons River Basin, India, using Sequential Uncertainty Fitting (SUFI-2) algorithm. *Modeling Earth Systems and Environment*, *3*(1), 30. <https://doi.org/10.1007/s40808-017-0306-z>
- Kumar, S., Singh, R. P., & Kalambukattu, J. G. (2021). Modeling daily surface runoff, sediment and nutrient loss at watershed scale employing Arc-APEX model interfaced with GIS: A case study in Lesser Himalayan landscape. *Environmental Earth Sciences*, *80*(15), 1–7.
- Kuti, I. A., & Ewemoje, T. A. (2021). Modelling of sediment yield using the soil and water assessment tool (SWAT) model: A case study of the Chanchaga Watersheds. *Nigeria. Scientific African*, *13*, e00936.
- Kwarteng, E. A., Gyamfi, C., Anyemedu, F. O. K., Adjei, K. A., & Anornu, G. K. (2021). Coupling SWAT and bathymetric data in modelling reservoir catchment hydrology. *Spatial Information Research*, *29*, 55–69.
- Lal, R. (2003). Soil erosion and the global carbon budget. *Environment International*, *29*(4), 437–450.
- Liu, Y. F., Dunkerley, D., López-Vicente, M., Shi, Z. H., & Wu, G. L. (2020). Trade-off between surface runoff and soil erosion during the implementation of ecological restoration programs in semi-arid regions: A meta-analysis. *Science of the Total Environment*, *712*, 136477.
- Luetzenburg, G., Bittner, M. J., Calsamiglia, A., Renschler, C. S., Estrany, J., & Poepl, R. (2020). Climate and land use change effects on soil erosion in two small agricultural catchment systems Fugnitz-Austria, Can Revull-Spain. *Science of the Total Environment*, *704*, 135389.
- Ma, L., Ascough, J. C., II., Ahuja, L. R., Shaffer, M. J., Hanson, J. D., & Rojas, K. W. (2000). Root Zone Water Quality Model sensitivity analysis using Monte Carlo simulation. *Transactions of ASAE*, *43*(4), 883–895.
- Mandal, D., Singh, R., Dhyani, S. K., & Dhyani, B. L. (2010). Landscape and land use effects on soil resources in a Himalayan watershed. *CATENA*, *81*(3), 203–208.
- Maurya, S., Srivastava, P. K., Yaduvanshi, A., Anand, A., Petropoulos, G. P., Zhuo, L., & Mall, R. K. (2021). Soil erosion in future scenario using CMIP5 models and earth observation datasets. *Journal of Hydrology*, *594*, 125851.
- Mondal, A., Khare, D., & Kundu, S. (2016). Impact assessment of climate change on future soil erosion and SOC loss. *Natural Hazards*, *82*(3), 1515–1539.
- Mondal, A., Khare, D., Kundu, S., Meena, P. K., Mishra, P. K., & Shukla, R. (2015). Impact of climate change on future soil erosion in different slope, land use, and soil-type conditions in a part of the Narmada River Basin, India. *Journal of Hydrologic Engineering*, *20*(6), C5014003.
- Morgan, R.P.C., Martin, L., Noble, C.A. (1986) *Soil erosion in the United Kingdom: a case study from mid-Bedfordshire*. Silsoe

- College Occasional Paper no. 14. Silsoe College, Cranfield Univ., Silsoe, UK.
- Moriassi, D. N., Arnold, J. G., Van Liew, M. W., Binger, R. L., Harmel, R. D., & Veith, T. (2007). Model evaluation guidelines for systematic quantification of accuracy in watershed simulations. *Transactions of the ASABE*, 50(3), 885–900.
- Morris, M. D. (1991). Factorial sampling plans for preliminary computational experiments. *Technometrics*, 27–33(2), 161–174.
- Mosbah, M., & Benabdallah, S. (2020). Assessment of land management practices on soil erosion using SWAT model in a Tunisian semi-arid catchment. *Journal of Soils and Sediments*, 20(2), 1129–1139.
- NAAS [National Academy of Agricultural Sciences] (2012). *Sustaining agricultural productivity through integrated soil management*. Policy paper no 56, National Academy of Agricultural Sciences, New Delhi, p 24.
- Narsimlu, B., Gosain, A. K., & Chahar, B. R. (2013). Assessment of future climate change impacts on water resources of Upper Sind River Basin, India using SWAT model. *Water Resources Management*, 27(10), 3647–3662.
- Narsimlu, B., Gosain, A. K., Chahar, B. R., Singh, S. K., & Srivastava, P. K. (2015). SWAT model calibration and uncertainty analysis for streamflow prediction in the Kunwari River Basin, India, using sequential uncertainty fitting. *Environmental Processes*, 2(1), 79–95.
- Neitsch, S.L., Arnold, J.G., Kiniry, J.R., Srinivasan, R., & Williams, J.R. (2002). *Soil and Water Assessment Tool user's manual, version 2000, Grassland*. Soil and Water Research Laboratory, Agricultural Research Service and Blackland Research Center, Texas Agricultural Experiment Station, Temple, Texas.
- Neitsch, S. L., Arnold, J. G., Kiniry, J. R., & Williams, J. R. (2011). *Soil and water assessment tool theoretical documentation version 2009*. Texas Water Resources Institute.
- Neitsch, S. L., Arnold, J. G., Kiniry, J. R., Williams, J. R., & King, K. W. (2005). *Soil and water assessment tool theoretical documentation grassland*. Soil and Water Research Laboratory. (p. 506p)
- Niazkar, M., & Zakwan, M. (2021). Assessment of artificial intelligence models for developing single-value and loop rating curves. *Complexity*. <https://doi.org/10.1155/2021/6627011>
- Osei, M. A., Amekudzi, L. K., Wemegah, D. D., Preko, K., Gyawu, E. S., & Obiri-Danso, K. (2019). The impact of climate and land-use changes on the hydrological processes of Owabi catchment from SWAT analysis. *Journal of Hydrology: Regional Studies*, 25, 100620.
- Pal, S. C., & Chakraborty, R. (2019). Simulating the impact of climate change on soil erosion in sub-tropical monsoon dominated watershed based on RUSLE, SCS runoff and MIROC5 climatic model. *Advances in Space Research*, 64(2), 352–377.
- Pal, S. C., Chakraborty, R., Roy, P., Chowdhuri, I., Das, B., Saha, A., & Shit, M. (2021). Changing climate and land use of 21st century influences soil erosion in India. *Gondwana Research*, 94, 164–185.
- Park, J. Y., Ale, S., Teague, W. R., & Jeong, J. (2017). Evaluating the ranch and watershed scale impacts of using traditional and adaptive multi-paddock grazing on runoff, sediment and nutrient losses in North Texas, USA. *Agriculture, Ecosystems & Environment*, 240, 32–44.
- Peel, M. C., Finlayson, B. L., & McMahon, T. A. (2007). Updated world map of the Köppen-Geiger climate classification. *Hydrology and Earth System Sciences Discussions*, 4, 439–473.
- Pijl, A., Reuter, L. E., Quarella, E., Vogel, T. A., & Tarolli, P. (2020). GIS-based soil erosion modelling under various steep-slope vineyard practices. *CATENA*, 193, 104604.
- Pimentel, D. (2006). Soil erosion: A food and environmental threat. *Environment, Development and Sustainability*, 8(1), 119–137.
- Prasannakumar, V., Vijith, H., Abinod, S., & Geetha, N. J. (2012). Estimation of soil erosion risk within a small mountainous watershed in Kerala, India, using Revised Universal Soil Loss Equation (RUSLE) and geo-information technology. *Geoscience Frontiers*, 1, 3(2), 209–215.
- Qiu, L. J., Zheng, F. L., & Yin, R. S. (2012). SWAT-based runoff and sediment simulation in a small watershed, the loessial hilly-gulied region of China: capabilities and challenges. *International Journal of Sediment Research*, 1, 27(2), 226–234.
- Raisi, M. B., Vafakhah, M., & Moradi, H. (2021). Modeling Snowmelt Runoff Under CMIP5 Scenarios in the Beheshtabad Watershed. *Iranian Journal of Science and Technology, Transactions of Civil Engineering*. <https://doi.org/10.1007/s40996-021-00687-8>
- Rajbanshi, J., & Bhattacharya, S. (2021). Modelling the impact of climate change on soil erosion and sediment yield: A case study in a sub-tropical catchment, India. *Modeling Earth Systems and Environment*, 7, 1–23.
- Richardson, C. W. (1985). Weather simulation for crop management models. *Transactions of ASAE*, 28, 1602–1606.
- Rivington, M., Miller, D., Matthews, K. B., Russell, G., Bellocchi, G., & Buchan, K. (2008). Evaluating regional climate model estimates against site-specific observed data in the UK. *Climatic Change*, 88(2), 157–185.
- Saharia, A. M., & Sarma, A. K. (2018). Future climate change impact evaluation on hydrologic processes in the Bharalu and Basistha basins using SWAT model. *Natural Hazards*, 92(3), 1463–1488.
- Salazar, S., Francés, F., Komma, J., Blume, T., Francke, T., Bronstert, A., & Blöschl, G. (2012). A comparative analysis of the effectiveness of flood management measures based on the concept of “retaining water in the landscape” in different European hydro-climatic regions. *Natural Hazards and Earth System Sciences*, 12(11), 3287–3306.
- Samaras, A. G., & Koutitas, C. G. (2014). Modeling the impact of climate change on sediment transport and morphology in coupled watershed-coast systems: A case study using an integrated approach. *International Journal of Sediment Research*, 29(3), 304–315.
- Shi, W., & Huang, M. (2021). Predictions of soil and nutrient losses using a modified SWAT model in a large hilly-gully watershed of the Chinese Loess Plateau. *International Soil and Water Conservation Research*, 9(2), 291–304.
- Simonneaux, V., Cheggour, A., Deschamps, C., Mouillot, F., Cerdan, O., & Le Bissonnais, Y. (2015). Land use and climate change effects on soil erosion in a semi-arid mountainous watershed (High Atlas, Morocco). *Journal of Arid Environments*, 122, 64–75.
- Singh, A. (2009). *Characterizing Runoff Generation Mechanism for Modelling Runoff and Soil Erosion in Small Watershed of Himalayan Region*. M. Tech. (RS & GIS) thesis. ITC.
- Singh, R.P. (2012). *Surface runoff, Soil erosion and Water Quality estimation using APEX model integrated with GIS—A case study in Himalayan Watershed*. M. Tech. (RS & GIS) thesis, Andhra University, Visakhapatnam, 98p.
- Singh, G., Babu, R., Narain, P., Bhushan, L. S., & Abrol, I. P. (1992). Soil erosion rates in India. *Journal of Soil and Water Conservation*, 47(1), 97–99.
- Singh, A. K., Kumar, S., & Naithani, S. (2021). Modelling runoff and sediment yield using GeoWEPP: a study in a watershed of lesser Himalayan landscape, India. *Modeling Earth Systems and Environment*, 7(3), 2089–2100.
- Sirikaew, U., Seeboonruang, U., Tanachaichoksirikun, P., Wattanasetpong, J., Chulkaivalsucharit, V., & Chen, W. (2020). Impact of Climate Change on Soil Erosion in the Lam Phra Phloeng Watershed. *Water*, 12(12), 3527.
- Sisay, E., Halefom, A., Khare, D., Singh, L., & Worku, T. (2017). Hydrological modelling of ungauged urban watershed using

- SWAT model. *Modeling Earth Systems and Environment*, 3(2), 693–702.
- Stefanidis, S., & Stathis, D. (2018). Effect of climate change on soil erosion in a mountainous mediterranean catchment (Central Pinus, Greece). *Water*, 10(10), 1469.
- Strahler, A. (1964). Quantitative geomorphology of drainage basins and channel networks. In V. T. Chow (Ed.), *Handbook of applied hydrology* (pp. 4-39-4–76). New York: McGraw-Hill.
- Suliman, A. H. A., Jajarmizadeh, M., Harun, S., & Darus, I. Z. M. (2015). Comparison of semi-distributed, GIS-based hydrological models for the prediction of streamflow in a large catchment. *Water Resources Management*, 29(9), 3095–3110.
- Swarnkar, S., Malini, A., Tripathi, S., & Sinha, R. (2018). Assessment of uncertainties in soil erosion and sediment yield estimates at ungauged basins: An application to the Garra River basin, India. *Hydrology and Earth System Sciences*, 22(4), 2471–2485. <https://doi.org/10.5194/hess-22-2471-2018>
- Tewari, V. P., Verma, R. K., & Von Gadov, K. (2017). Climate change effects in the Western Himalayan ecosystems of India: evidence and strategies. *Forest Ecosystems*, 4(1), 1–9.
- Tiwari, P. (2008). Land use changes in Himalaya and their impacts on environment, society and economy: A study of the Lake Region in Kumaon Himalaya, India. *Advances in Atmospheric Sciences*, 25(6), 1029.
- Trocine, L., & Malone, L. C. (2000, December). Finding important independent variables through screening designs: a comparison of methods. In *2000 Winter simulation conference proceedings (Cat. No. 00CH37165)* (Vol. 1, pp. 749–754). IEEE.
- Trotochaud, J., Flanagan, D. C., & Engel, B. A. (2016). A simple technique for obtaining future climate data inputs for natural resource models. *Applied Engineering in Agriculture*, 32(3), 371–381.
- USDA-SCS [U.S. Department of Agriculture-Soil Conservation Service], (1972) SCS National Engineering Handbook, Section 4, Hydrology. Chapter 10, Estimation of Direct Runoff from Storm Rainfall. U.S. Department of Agriculture, Soil Conservation Service, Washington, D.C., pp. 10.1–10.24.
- van Griensven, A., & Bauwens, W. (2003). Multiobjective autocalibration for semidistributed water quality models. *Water Resources Research*, 39(12), 1348–1356.
- Van Liew, M. W., Arnold, J. G., & Bosch, D. D. (2005). Problems and potential of autocalibrating a hydrologic model. *Transactions of ASAE*, 48(3), 1025–1040.
- Wilby, R. L., & Dawson, C. W. (2004). Using SDSM version 3.1—A decision support tool for the assessment of regional climate change impacts. User manual, 8.
- Wischmeier, W. H., Johnson, C. B., & Cross, B. V. (1971). Soil erodibility nomograph for farmland and construction sites. *Journal of Soil and Water Conservation*, 26, 189–193.
- Wuepper, D., Borrelli, P., & Finger, R. (2020). Countries and the global rate of soil erosion. *Nature Sustainability*, 3(1), 51–55. <https://doi.org/10.1038/s41893-019-0438-4>
- Yaduvanshi, A., Zaroug, M., Bendapudi, R., & New, M. (2019). Impacts of 1.5 C and 2 C global warming on regional rainfall and temperature change across India. *Environmental Research Communications*, 1(12), 125002.
- Yang, D., Kanae, S., Oki, T., Koike, T., & Musiak, K. (2003). Global potential soil erosion with reference to land use and climate changes. *Hydrological Processes*, 17(14), 2913–2928.
- Yin, L., Wang, X., Pan, J., & Gassman, P. W. (2009). Evaluation of apex for daily runoff and sediment yield from three plots in the middle Huaihe river watershed, China. *Transactions of the ASABE*, 52(6), 1833–1845.
- Zhang, H., Wang, B., Li Liu, D., Zhang, M., Leslie, L. M., & Yu, Q. (2020). Using an improved SWAT model to simulate hydrological responses to land use change: A case study of a catchment in tropical Australia. *Journal of Hydrology*, 585, 124822.
- Zhao, X., Huang, J., Wu, P., & Gao, X. (2014). The dynamic effects of pastures and crop on runoff and sediments reduction at loess slopes under simulated rainfall conditions. *CATENA*, 119, 1–7.
- Zheng, J. J., Xiu-Bin, H. E., Walling, D., Zhang, X. B., Flanagan, D., & Yong-Qing, Q. I. (2007). Assessing soil erosion rates on manually-tilled hillslopes in the Sichuan Hilly Basin Using 137Cs and 210Pbex measurements. *Pedosphere*, 17(3), 273–283.

Publisher's Note Springer Nature remains neutral with regard to jurisdictional claims in published maps and institutional affiliations.